Modelling and predictions of time-dependent local stress distributions around cracks under dwell loading in a nickel-based superalloy at high temperatures

Florence M. Muller [a,1,*]

Chizhou Fang [b,*], Hector C. Basoalto [b], Steve Williams [c], Paul Bowen [a]

[a] School of Metallurgy and Materials, University of Birmingham, Edgbaston, Birmingham B15 2TT, United Kingdom

[b] Department of Materials Science and Engineering, University of Sheffield, Mappin St, Sheffield S1 3JD, United Kingdom

[c] Institute of Structural Materials, Swansea University, Swansea SA1 8EN, United Kingdom

* Corresponding authors:

Florence M. Muller

FlorenceMarie.Muller@ugent.be

Chizhou Fang

c.fang@sheffield.ac.uk

[1] Medical Image and Signal Processing (MEDISIP, ELIS, IBiTech), Faculty of Engineering and Architecture, Campus Ghent University Hospital (Entrance 36), Corneel Heymanslaan, Gent 9000, Belgium (present affiliation)

Abstract

Finite element (FE) analysis modelling of crack configurations was used to provide insights into the role of time-dependent deformation on dwell fatigue crack growth (DFCG) in turbine disc alloys. In particular, the potential influence of time-dependent deformation on fatigue crack growth rates observed during dwell holding periods and the potential crack growth retardation phenomena that can occur for overload-dwell cycles were investigated. The FE model evaluated the mechanical stress state evolution in a two-dimensional cracked geometry subjected to standard dwell and overload-dwell stress waveforms for a given microstructural condition (based on its γ' particle distribution). Crack-opening stress distributions as a function of dwell time and distance ahead of the crack-tip were interrogated, with the aim to investigate the potential influence of local crack-tip stresses on crack growth during dwell holding periods and the potential for crack growth retardation following overload cycles. Stress distribution profiles predicted by dwell-only simulations showed how quickly local crack-tip stresses relax due to time-dependent plasticity. Characteristic effects of overloads of dwell crack growth resistance observed in experiments were also reasonably well captured. A numerically-derived incubation time was successfully applied in predicting the general trends of achieving more pronounced retardation effects with larger overload factors and extended periods of overloading prior to periods of dwell. FE modelling predicted a significant difference in behaviour between an overload for a given overload factor with a hold time at peak load of 1s and 10s. This study emphasises the importance of studying local crack-tip stresses in regards to characterising DFCG behaviour of turbine disc alloys.

Keywords

Dwell fatigue crack growth, Finite element modelling, Nickel-based turbine disc alloys, Overload, Time-dependent plasticity

1. Introduction

Gas turbine development drives to optimise engine performance and efficiency by pushing new generation disc alloys (powder metallurgy nickel-based superalloys) to increasing levels of operating temperature regimes [1, 2]. At high temperatures (>500°C) in air, a mechanism of brittle intergranular dwell fatigue crack growth (DFCG) is observed and has been discussed as being influenced by several interacting and (often) competing contributions of: (i) cyclic plastic deformation; (ii) time (and stress)-dependent oxide formation and/or oxygen embrittlement of grain-boundaries (GB); and (iii) time-dependent plasticity (creep deformation) [3-6]. Such brittle intergranular fracture occurs in air, but not in vacuum. At the highest temperatures (typically above 750°C) the intergranular crack growth mechanism transitions to creep fracture by intergranular micro-void coalescence, which can now occur in both air and in vacuum. Since such brittle intergranular mechanisms in loading cycles with long dwell periods can give crack growth rates (CGR) that are markedly higher than those observed for transgranular crack growth in fast loading cycles, DFCG in Ni-based superalloys has potential to become one limiting factor on a declaration of certified life for turbine disc applications. **Fig. 1** illustrates three loading waveforms commonly used to simulate representative engine loading cycles.

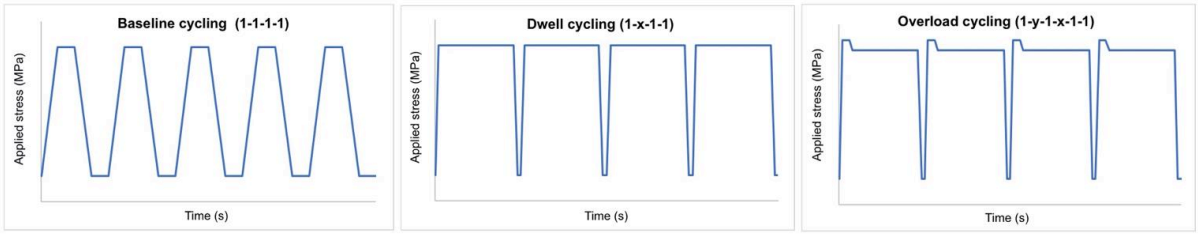

Fig. 1: Three examples of typical engine loading cycles: baseline cycling, dwell cycling and overload cycling.

Oxidising environments have long been recognised to cause significant increases FCGR per cycle, especially when introducing dwell periods at peak load, as a result of intergranular crack growth (**Fig. 2**) [7-10]. Intergranular failure modes and accelerated FCGR are primarily controlled by oxygen/oxide damage effects at and/or very close to the growing crack-tip [6, 11-13]. Stress-assisted

grain-boundary oxidation (SAGBO) is widely accepted as the dominant mechanism accounting for the detrimental influence of oxygen on DFCG behaviour [14-16]. Under combined conditions of high stress and temperature, the preferential (and accelerated) formation and growth of an oxide intrusion along a GB ahead of the crack-tip results in GB fracture, thereby increasing CGR with oxide failure. When crack growth tests are repeated in vacuum, dwell effects are almost completely eliminated [3, 9, 10, 12], unless the temperature is high enough (>750°C) for creep crack growth processes (intergranular micro-void coalescence) to be activated [16, 17].

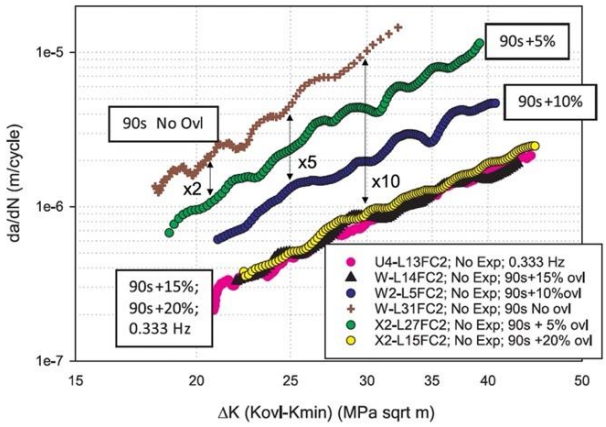

Fig. 2: Crack growth resistance curves (da/dN vs ΔK_{full}) showing an example of dwell and overload-dwell effects on DFCG behaviour in LSHR alloy at 704°C [18].

Much previous research has focused on studying the relative significance of creep damage and environmental degradation on crack-tip damage. However, a full description of DFCG behaviour needs to account for stress relaxation effects occurring in the vicinity of the crack-tip, particularly during prolonged dwell periods. Stress relaxation will reduce elevated tensile stresses local to the crack-tip. If a stress-controlled fracture criterion is invoked for oxide (or embrittled GB) cracking, then this relaxation (due to time-dependent (creep) deformation) might have the potential to retard intergranular crack growth. A complete analysis of any oxide cracking mechanism will also consider potential effects of the oxide putting itself into compression as it grows (due to a volumetric expansion upon formation) as shown schematically in **Fig. 3** [14, 19]. In this current paper, emphasis is put on understanding and predicting time-dependent plasticity which will promote near-tip stress relaxation (due to the

accumulation of creep strain) and concomitant crack-tip blunting which may have the potential to reduce the rate of oxide cracking [17, 18]. Given the opposing effects over time (within any dwell period) of environmental degradation (increased oxide growth and/or GB embrittlement expected to accelerate DFCGR) and near-tip stress relaxation (which may decrease DFCGR) [6, 16, 20] it is useful to decouple the effects of creep deformation and oxidation to provide further insight on the separate action of these local mechanisms. So, this current paper considers stress relaxation effects arising from time-dependent plasticity only.

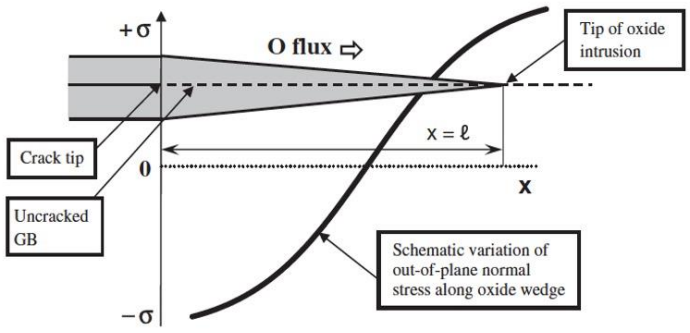

Fig. 3: Schematic illustration showing the variation in normal out-of-plane stress along oxide intrusion ($0 \leq x \leq l$) in the absence of an applied load [14].

The introduction of an overload segment prior to dwell periods may result in further significant reductions of FCGR compared to (otherwise similar) dwell-only cycling, with overload effects usually being interpreted in terms of transient changes to local crack-tip plasticity. However, within this field, relatively few studies have been reported in the scientific literature [9, 13, 18, 21-23]. For severe overload conditions, it has been observed that damaging dwell effects can be eliminated entirely, with growth rates decreasing down to levels of baseline loading (fatigue crack growth) (**Fig. 2**) after [18]. These dramatic effects of suppressed or retarded crack growth have been rationalised by significant variations in near-tip stress relaxation response [21, 22]. Stress relaxation at the crack tip will be beneficial provided that the influence from lower stresses and crack tip blunting is greater than any potential debit from accumulating higher levels of creep strain. The complexity of this crack growth retardation reinforces the motivation here to analyse effects of time-dependent plasticity alone.

The need for more detailed physical insight on DFCG behaviour of turbine disc alloys has driven the application of FEA modelling of crack configurations. Both a comprehensive mesh formulation and a detailed numerical creep model (based on microstructural variables) were available from previous work by some of the current authors [19]. The model here considers constitutive equations for material creep and plasticity alone (while the original model also includes effects of oxidation and oxide growth). By decoupling the effects of oxidation and plasticity, this modelling work focuses on the underlying mechanism of stress relaxation due to time-dependent plasticity and studies crack-opening stress modifications in the vicinity of the crack-tip to characterise DFCG behaviour of Ni-based superalloys. This paper describes the FE method used to evaluate the mechanical stress state evolution in a 2D cracked geometry subjected to standard dwell and overload stress waveforms for a given microstructural condition (γ' particle distributions) somewhat typical of the distributions applicable to the proprietary alloy RR1000. The primary purpose of this paper is to investigate the potential influence of local crack-tip stresses on crack growth during dwell holding periods and the potential for crack growth retardation following overload cycles. It is limited here to a time-dependent stress field analysis of a stationary crack and it does not incorporate any node release schemes to simulate crack advance.

2. Materials and Methods

2.1. Numerical implementations

2.1.1. *The Finite Element model*

The geometry of the FE model used in this study, a 10x10 mm^2 cross-sectional area representative of the single-edge notched tension (SENT) specimen geometry, is shown in **Fig. 4** . The use of plane-strain elements is consistent with a knowledge that the individual crack growth mechanism to which the current FE model outputs will be applied occurs more readily away from plane stress regions. For computation efficiency, the global model includes a coarse mesh away from the crack and a fine mesh of 25 nm size elements near the crack-tip which is needed to obtain accurate stress states locally. The

justification for using such a refined local mesh is rationalized in view of the scale of the envisaged crack growth increments and is discussed later.

The boundary conditions are also shown in **Fig. 4**. AB represents a 2 mm stationary crack. BC denotes the GB ahead of the crack-tip defined by a symmetry boundary condition in order to account for the material contact that prevents vertical displacement. Point B represents the crack-tip and point C is restrained. The applied stress acts on the top surface ED which is allowed to deform freely under this pressure loading.

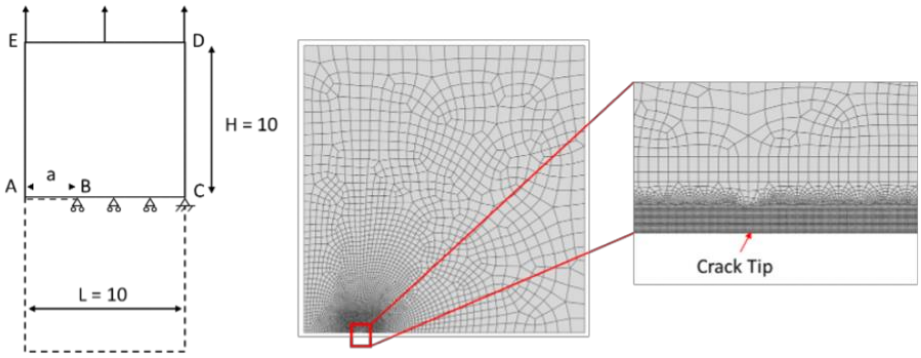

Fig. 4: Schematic of the boundary conditions applied to the 2D SENT specimen geometry. Illustration of the implemented 2D FE mesh in ABAQUS. Global mesh with coarse mesh and a locally refined mesh near the crack-tip.

2.1.2. *The Finite Element mesh*

The FE mesh used here is constructed using a local refined mesh near the crack-tip (with element size of 25 nm) and a coarser mesh away from the crack-tip, as shown in **Fig. 4**. The necessity for a refined mesh locally can be justified in terms of the local mechanisms envisaged. That the physical length scales actually involved here are on an action zone very local to the crack-tip as can be appreciated both in terms of crack growth per dwell cycle where: for one-hour dwell testing at 650°C in air, FCGR in RR1000 are found experimentally to be around 0.03-0.04 mm/cycle which is roughly equivalent to 8-11 nm/s for values of K (ΔK) of 20-30 MPa.m1/2 [9]; and in terms of oxide growth: ahead of stationary cracks, where oxides can grow to about 4.5 µm when exposed under a constant load (stress intensity factor) for 5hrs [15] (which can be estimated on a linear basis with time to be 15 nm/s).

2.1.3. *Material model and microstructure*

The high-temperature strength of Ni-based superalloys (of a given grain size) is primarily derived from the distribution of strengthening γ' particles which disrupt continuous glide of dislocations. Pinned dislocations overcome γ' particles through local climb and creep can be treated as a jerky glide process, with climb and glide events happening simultaneously [24, 25]. The mechanical creep behaviour is therefore most suitably represented by a constitutive model that connects microstructure and macroscopic creep rate. Dyson [26] derived a microstructure-explicit state variable approach for uni-modal precipitate-strengthened alloys. Basoalto *et al.* [27-29] extended the dispersion-controlled creep model developed by Dyson [26] to account for multi-modal γ' distributions. For this type of extended creep model, the constitutive equations are explicitly expressed in terms of quantitative measures of initial microstructural features and their subsequent rates of evolution. Details can be found elsewhere [19] but it is noted that the model parameters have been optimised by extensive correlations with experimental data and the output of such correlations are reproduced in **Table 1**.

The microstructure-explicit visco-plastic model established by Basoalto has been adopted in the present modelling work to describe the mechanical material behaviour of a standard heat-treated microstructure typical of that to be found in fine-grained RR1000. The commercial FE software ABAQUS is used for performing non-linear static stress analyses. Constitutive laws are implemented and numerically solved in an ABAQUS user-defined subroutine (UMAT) [19, 30] . In this study, spatial-temporal evolution of the multi-modal γ' size distribution is not considered. The associated microstructural model input are the γ' dispersion parameters, i.e. volume fraction and mean size of primary, secondary and tertiary γ'. Creep rates scale with volume fraction of γ' precipitates and there is non-linear scaling with inter-particle distances (which means the higher the number density of particles, the smaller the spacing and hence the lower the creep rates). Controlling the creep rates with particle dispersion is essential for controlling the stress relaxation ahead of the crack-tip which in turn influences DFCG behaviour. Grain size distribution effects are neglected based on the assumption that creep deformation is controlled by interparticle distances and not grain dimensions. Since this creep model

does not contain any dependency on grain size, it is applicable to situations around crack-tips where local stresses are high, and deformation will be dominated by dislocation activity alone This, however, implies that any hardening behaviour of flow stresses (Hall-Petch type) will not be captured. The γ' particle distributions considered in the present paper are given in **Table 2**. They are representative of distributions that may occur in fine-grained variants of the RR1000 alloy.

Table 1: Microstructural model parameters used in the constitutive model [19, 27].

Burger vector, b (m)	2.54×10^{-10}
Taylor factor, M	3.1
Dislocation multiplication parameter, C	100
Activation energy, Q (kJ.mol^{-1})	305
Pre-exponential diffusivity, D_0 (m^2.s^{-1})	1×10^{-5}
Jog density, c_j	1
Mobile dislocation density, ρ_m (m^{-2})	10^{10}
Misfit stress (MPa)	-120
Young's Modulus (GPa)	188
Poison's ratio	0.33

Table 2: Volume fraction and average diameter size of primary, secondary and tertiary γ' for a simulated (fine-grained) RR1000 microstructure.

Primary γ'	Volume fraction, V_{f1}	12 %
Secondary γ'	Volume fraction, V_{f2}	28 %
	Average size, $\emptyset_2$	120 nm
Tertiary γ'	Volume fraction, V_{f3}	5 %
	Average size, $\emptyset_3$	20 nm
Total volume fraction of γ'		45 %

2.1.4. *Loading waveforms and simulated conditions*

Within the scope of this project, the simulations explore the mechanical stress fields near a stationary crack-tip as a function of time-dependent plasticity. For a stationary 2 mm crack, applied far-field stresses of 200 and 300 MPa give linear elastic stress intensity factors of 21.7 and 32.6 MPa.m$^{1/2}$

respectively using Equ.(1) where the "compliance" C for a SENT specimen is given as a function of a/W [31] in Equ.(2).

$$K_I = C\,\sigma\,(\pi a)^{1/2} \tag{1}$$

$$C = 1.12 - 0.231\left(\frac{a}{W}\right) + 10.55\left(\frac{a}{W}\right)^2 - 21.72\left(\frac{a}{W}\right)^3 + 30.39\left(\frac{a}{W}\right)^4 \tag{2}$$

Dwell and overload loading waveforms are programmed as stress-time histories (but are guided in all cases by previous experiments and/or envisaged by potential in-service loading). Appropriate time step resolution definitions allow the time history to be split into smaller suitable time increments in order to evaluate the stress state at each node at determined moments in time. The model is run under plane-strain and isothermal conditions. Each condition is modelled by applying a single stress cycle, neglecting the influence of any previous loading history and the simulation stops at the point of unloading from dwell to minimum stress. The dwell-only waveform (1-t_{dwell}) is implemented by two separate loading segments (**Fig. 5(a)**). The overload dwell waveform (1- t_{OL} -1- t_{dwell}) is defined by four loading segments (**Fig. 5(b)**). To replicate the variation in stress with time during an overload, an amplitude curve based on tabular data is implemented. The magnitude of overload is defined by an overload factor (OLF) as follows, $\sigma_{OL}/\sigma_{dwell}$. Note that for OLF = 1.0 no overload is applied, and the cycle reduces to the dwell-only waveform. The influence of nominal dwell stress (σ_{dwell}), dwell time (t_{dwell}), overload factor (OLF) and overload hold time (t_{OL}) are studied. Loading waveforms are simulated for subsequent dwell periods of 30, 120, 300, 600, 1200 and 3600 seconds. Overload factors of 1.05 and 1.15, and overload hold times of 1 and 10 seconds are considered in this paper.

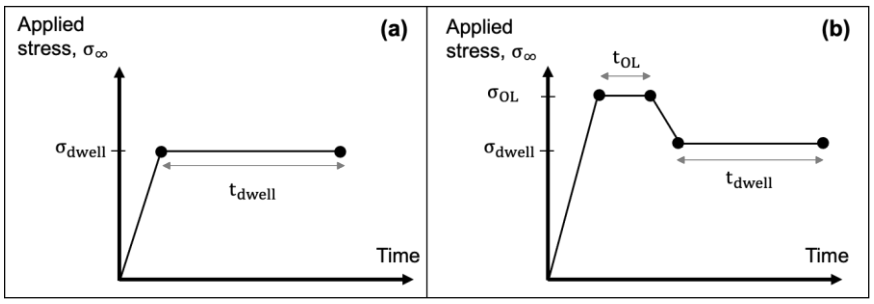

Fig. 5: Simulated loading waveforms **(a)** Standard dwell cycle is modelled as 1-t_{dwell} stress waveform: initial stress ramp-up to σ_{dwell} in 1s (t_1) and hold at σ_{dwell} for t_{dwell}. **(b)** Overload cycle is modelled as 1-t_{OL}-1-t_{dwell} stress waveform: initial stress ramp-up to σ_{OL} in 1s (t_1), hold at overload until t_2 (t_2 - t_1 denotes the overload dwell time), unload from σ_{OL} to σ_{dwell} in 1s (t_3) and normal hold at σ_{dwell} for t_{dwell}.

2.2. Data analysis

In the current paper, a stress-based approach was adopted to investigate crack-opening stress (σ_{22}) distributions as a function of dwell time and distance ahead of the crack-tip. The analysis specifically focused on local crack-tip stress fields and how these evolved during dwell (hold) periods when subjected to a standard dwell condition (STD) compared to an overload condition (OL). To generate spatial stress profiles, stress data was extracted from the local nodes and elements that, ahead of the modelled crack-tip, defined the plane containing the crack. One readily understood physically based approach for characterising near crack-tip behaviour uses the crack-tip opening displacement (CTOD) parameter. A sharp crack blunts initially on loading [32] and then it may also potentially blunt further under dwell (over time) with an external (far-field) load applied to the geometry. Thus, specifically for dwell-only simulations, the variation in CTOD as a function of time was investigated. To do this, a crack-tip opening node (CTO-node) was chosen 2 μm behind the crack-tip and examined in terms of its spatial vertical displacement. Note that this node was selected since it is close to the blunted crack-tip, yet one of the first nodes which will only suffer vertical displacement with further opening.

To consider a quantitative assessment of the effect of overloads on crack-opening stress fields, an engineering approximation was introduced to derive an incubation time which can be related to the potential for crack growth retardation following overload cycles, and which then leads to an effective dwell time (applied dwell time minus incubation time). Numerical outputs of σ_{22} with dwell time after

overloading were interrogated at the very first node (5 nm) ahead of the crack-tip and compared against the local stresses due to (non-overload) dwell times alone. This emphasises the importance of a local crack-tip stress criterion, but outputs of local stress profiles with time at a distance of up to 120 μm ahead of the crack-tip are also presented for selected cases.

3. Results: Application of the model

3.1. Standard dwell simulations

Stress-distance profiles predicted by the constitutive creep model using the multi-modal γ' microstructure listed in **Table 2** have been computed for dwell-only (standard) loading waveforms at 650°C. **Fig. 6** compares the crack-tip opening stress (S22) distribution at six different dwell times ranging from 30 to 3600 seconds for σ_{dwell} of 300 MPa. The stress-distance profile presented in **Fig. 6** is also shown with S22 normalised by the yield stress ($S22/\sigma_y$). Based on [19], the predicted average yield stress of the material (RR1000) is approximately 1000 MPa. During initial loading, the model predicts plasticity to occur close to the crack-tip, whereby the stress relaxes to approximately 3700 MPa at the crack-tip. When σ_{dwell} is first reached at t = 1s (during initial loading), dwell effects are not yet considered. Stress-distance curves demonstrate an overall reduction in σ_{22} with longer hold times, especially in the vicinity of the crack-tip. Significant stress relaxation notably arises within just a few tens of seconds into the dwell. However, beyond a certain distance away (0.07 mm for σ_{dwell} = 200 MPa; 0.18 mm for σ_{dwell} = 300 MPa) from the crack-tip, all profiles collapse into a single curve and re-join the t = 1s (initial loading) curve. General trends suggest that major changes to time-dependent plasticity occur in local regions very close to the crack-tip (typically within 20 μm).

Crack-opening stress distributions feature a local peak at a short distance away from the crack-tip. The magnitude of this maximum σ_{22} is predicted both to decrease and to move further ahead of the crack-tip with increasing hold (dwell) times (**Table 3**). The distance is expressed here as the distance over which tensile stress levels exceed 95% of this peak. With longer dwell times (and higher applied K levels), local tensile stresses within 95% of the peak stress extend over a larger distance from the

crack-tip. Similar to the original time-independent plasticity analysis of McMeeking [32], the magnitude of the maximum σ_{22} does not vary significantly with different values of applied K.

Fig. 7 shows the variation in CTOD as a function of time. Note that the computed values of CTOD denote only half of the actual CTOD because of modelling geometry symmetry. The initially very sharp crack blunts, with CTOD values for initial loading (at t = 1s) of 0.6 and 1.2 μm (for a σ_{dwell} of 200 and 300 MPa respectively). This CTOD value then increases further and appears to be levelling out to 0.74 and 1.68 μm over the subsequent one-hour dwell period (for σ_{dwell} of 200 and 300 MPa).

Table 3: Tabular data of maximum crack-opening stress (σ_{22}) and corresponding distance covering 95% of this peak ($d_{95\%}$). Results are presented for initial loading (at t = 1s) and different dwell times with σ_{dwell} = 200 and 300 MPa.

		Initial loading (t = 1s)					
Applied dwell stress σ_{dwell} (MPa)		200			300		
Maximum σ_{22} (MPa)		4775			4740		
		Dwell time (s)					
		30	120	300	600	1200	3600
200 MPa (21.7 MPa.m$^{1/2}$)	Maximum σ_{22} (MPa)	3340	3060	2895	2780	2670	2490
	$d_{95\%}$ (μm)	2.6	3.5	4.5	4.9	5.3	7.3
300 MPa (32.6 MPa.m$^{1/2}$)	Maximum σ_{22} (MPa)	3360	3020	2865	2750	2635	2460
	$d_{95\%}$ (μm)	4.5	9.2	10.3	11.6	13.3	15.2

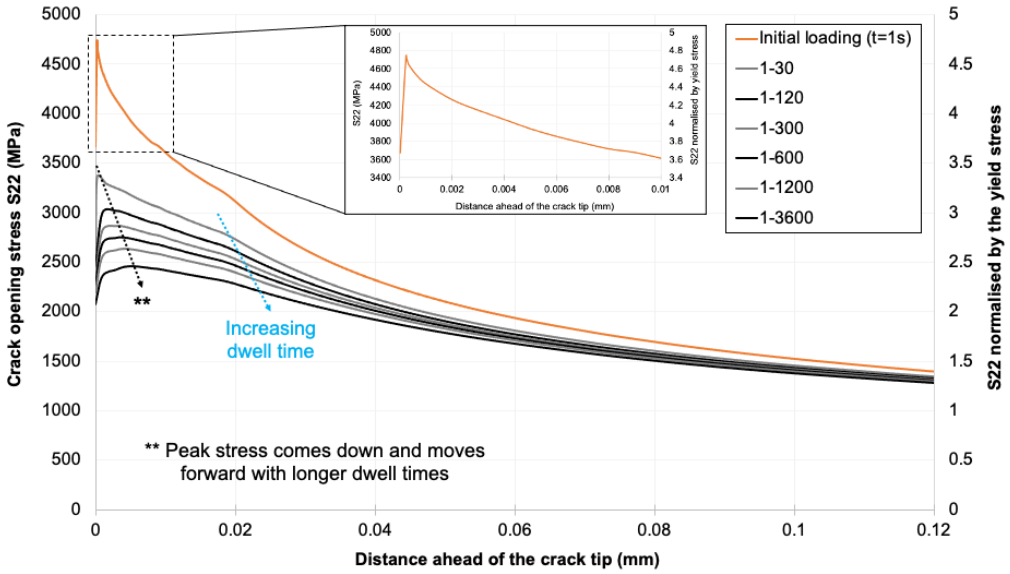

Fig. 6: Stress-distance profiles at different points for the FE model (RR1000 at 650°C) subjected to simulated dwell-only cycles with σ_{dwell} of 300 MPa. Stress distribution plotted in regards to crack-tip opening stress S22 and S22 normalised by the yield stress (σ_y = 1000 MPa).

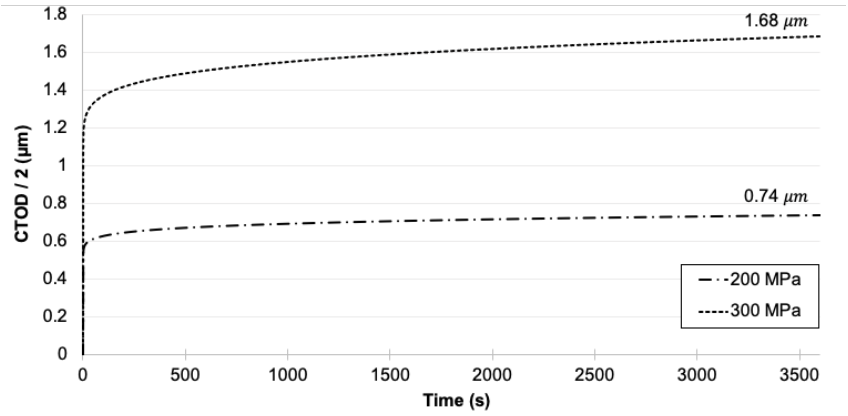

Fig. 7: Crack-tip opening displacement plotted versus time, with CTOD/2 numerically investigated at the CTO-node selected (2 μm behind the crack-tip).

3.2. Overload simulations

Four combinations of overload factors and overload dwell times (**Table 4**) were applied to the FE model. Each simulation was conducted at 650°C with σ_{dwell} of 200 and 300 MPa, matching K values of 21.7 and 32.6 MPa.m$^{1/2}$ respectively.

Table 4: Overview of the four simulated overload conditions varying in applied overload factor (OLF) and overload dwell time (t_{OL}).

Condition	1	2	3	4
OLF	1.05	1.15	1.05	1.15
t_{OL} (s)	1	1	10	10

Fig. 8 illustrates the stress-distance profiles generated at different time points for the OL condition 3 (OLF = 1.05, t_{OL} = 10s) simulated with σ_{dwell} of 300 MPa. Upon initial loading (at t_1 = 1s when σ_{OL} is first reached) the stress distribution (in orange) features similar characteristics to dwell-only (standard) stress profiles. Local crack opening stresses peak at short distance ahead of the crack-tip with a steep decrease in stress levels towards the crack-tip. Note that also here (as observed in behaviour during dwell-only loading) the constitutive response is modelled through a microstructure explicit rate-dependent formulation, resulting in stress relaxation ahead of the crack tip. However, upon partially unloading from the overload condition (σ_{OL} to σ_{dwell}), stress-distance profiles change significantly in shape with σ_{22} reducing preferentially close to the crack-tip. Therefore, reductions in local tensile stresses immediately ahead of the crack-tip are markedly larger than the percentage of unloading applied. **Fig. 8** also highlights that, in particular, near crack-tip stresses change appreciably with dwell time, while stress fields further away/ahead from the crack-tip (distance > 2 μm) are relatively flat with subtle differences only in σ_{22} for different hold (dwell) times.

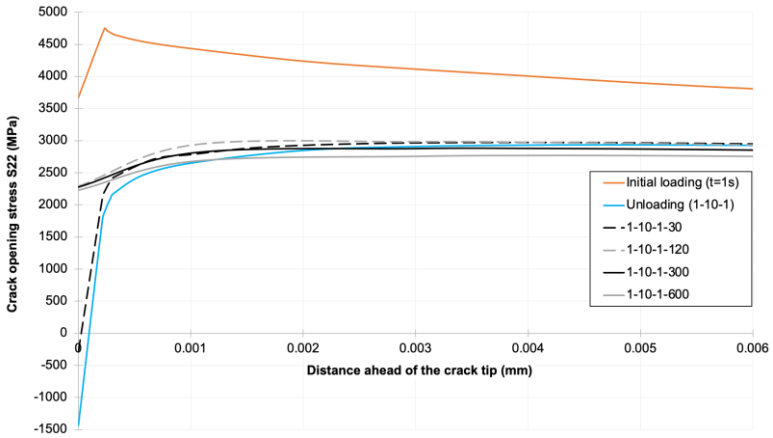

Fig. 8: Stress-distance profiles at different dwell times for the FE model subjected to σ_{dwell} = 300 MPa, OLF = 1.05 and t_{OL} = 10s.

Fig. 9 compares local crack-tip opening stress fields as a function of distance (up to 2 μm ahead of the crack-tip) for simulations run under: standard (STD) dwell; 1s OL; and 10s OL loading conditions with σ_{dwell} = 300 MPa and OLF = 1.05. Each graph (a-c) is plotted for a specific dwell time (30, 120 and 300s respectively) and, in each case, local stress-distance profiles for the three different loading conditions can be compared at similar moments in time. For t_{dwell} = 30s (**Fig. 9(a)**), neither 1s nor 10s OL stress curves (1-1-1-30 and 1-10-1-30) have re-joined the STD dwell curve (1-30). For both OL conditions, near-tip stresses are recovering towards their non-overload level with σ_{22} even being compressive for 1-10-1-30 (-280 MPa at the crack-tip). For t_{dwell} = 120s (**Fig. 9(b)**), local stress states associated to 1-120 and 1-1-1-120 are now predicted to be essentially identical (at the crack-tip: 2455 and 2450 MPa respectively). In contrast for 1-10-1-120, tensile stress levels are still appreciably lower (2290 MPa). The effect of overloads on near-tip stress recovery seems to reduce more gradually for t_{OL} = 10s compared to t_{OL} = 1s. At t_{dwell} = 300s (**Fig. 9(c)**), all three stress curves have converged and local crack-tip stress fields for 10s OL appear to have now also fully recovered back to their "unloaded state". These results suggest that, during a first portion of subsequent dwell time, local crack-tip stresses from simulated OL cycles relax back towards their standard dwell (non-overload) stress state, whilst neighbouring stress fields redistribute. However, with longer hold times, crack-tip stress recovery diminishes as local stress states converge, and thereafter normal dwell effects will resume (i.e. σ_{22} profiles are progressively lowered with prolonged dwell).

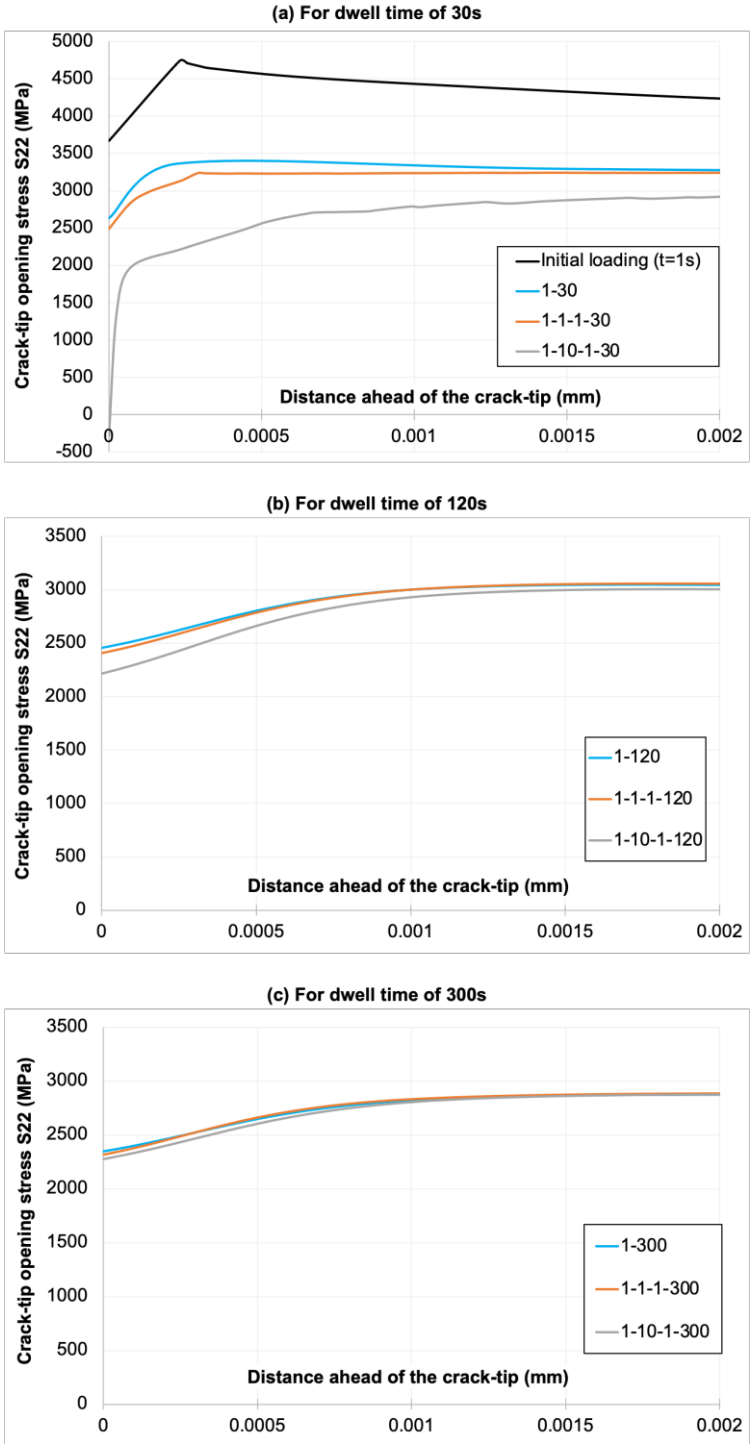

Fig. 9: Local stress-distance profiles compared for standard dwell, 1s and 10s overload condition (σ_{dwell} = 300 MPa and OLF = 1.05) (a) t_{dwell} = 30s, (b) t_{dwell} = 120s, (c) t_{dwell} = 300s.

To characterise the entire local crack-tip stress field evolution with dwell time, crack-opening stresses are tracked against time at an individual node very close to the crack-tip. Here, the first node ahead of the modelled crack-tip (5 nm away) was chosen. Since this node is very local to the crack-tip,

stress data extracted from this node is presumed to characterise crack-opening stress levels essentially at the crack-tip. **Fig. 10** represents the crack-tip stress-time histories generated for all four simulated OL conditions and compares them against the standard dwell relaxation curve (in red). Note that the time axis captures the onset of non-overload dwell allowing stress-time histories to be compared at similar times during subsequent dwell. At the start of dwell, crack-tip σ_{22} predicted for OL simulations are markedly lower, or as is the case for some conditions approach zero, or even become strongly compressive (-3700 MPa). Over time, these local crack-tip stress fields slowly relax back towards normal dwell stress levels.

There is a prominent difference in how quickly local tensile stresses recover back to their non-overload level, strongly dependent on both OLF and t_{OL}. For illustrative purpose, an engineering approximation is next adopted to introduce an incubation time (t_{inc}) defined as the time it takes upon unloading for crack-tip stresses at this node to recover to within 2% of the local stress at this node under relaxation from a standard dwell hold. Numerically-derived incubation times (**Table 5**) increase with higher OLF and longer t_{OL}. Extended OL dwell (10s) as well as larger OL (15%) produce larger compressive stress fields close to the crack-tip and so it takes longer for stresses to recover back which translates into increased t_{inc}. Note that higher values of K result in slightly shorter t_{inc} which implies a slightly reduced OL effect. Modelling even predicts that for OL No. 4 condition (OLF = 1.15 and t_{OL} = 10s) crack-tip σ_{22} will never fully recover even after a one-hour dwell cycle.

Table 5: Incubation times, as captured by FE simulations, are presented for all four overload conditions simulated for two different applied K values

Condition	**1** t_{OL} = 1s OLF = 1.05	**2** t_{OL} = 1s OLF = 1.15	**3** t_{OL} = 10s OLF = 1.05	**4** t_{OL} = 10s OLF = 1.15
t_{inc} (s) for K = 21.7 MPa.m$^{1/2}$	40	2540	290	>3,600
t_{inc} (s) for K = 32.6 MPa.m$^{1/2}$	25	1430	240	>3,600

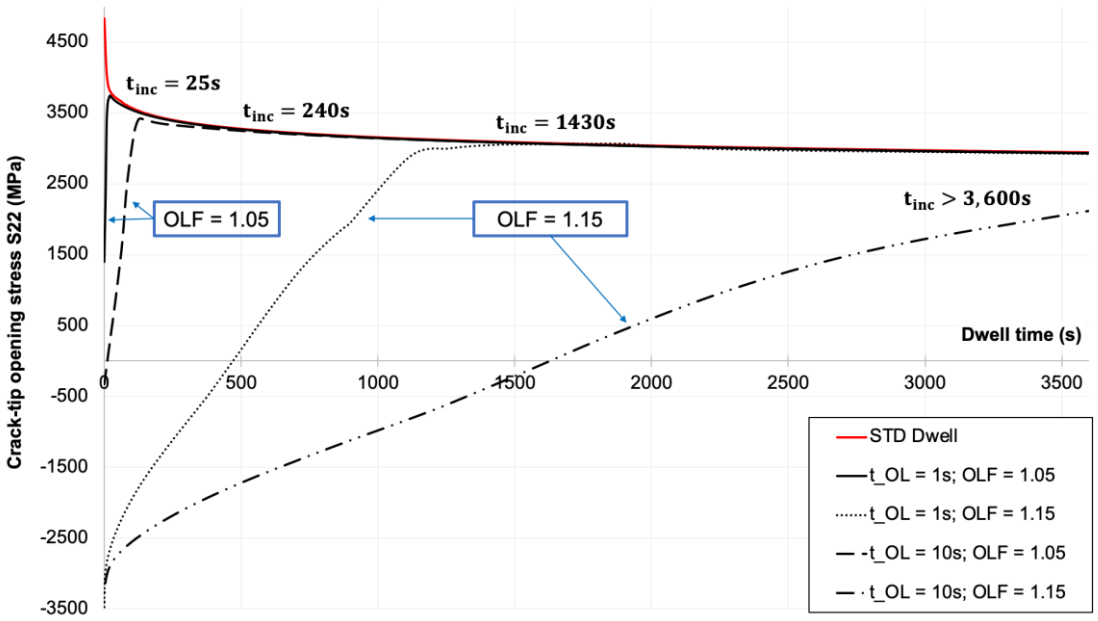

Fig. 10: Crack-tip stress-time histories (σ_{22} versus non-overload dwell time) are generated at the first node ahead of the modelled crack-tip and compare four different overload conditions with the standard (STD) dwell loading case (for σ_{dwell} = 300 MPa).

4. Discussion

Although crack growth testing has led to the development of empirically-based predictive models, research has not been able to produce many conclusive results on local crack-tip phenomena involved during failure mode interactions of cycle- and time-dependent processes [3, 5, 6]. Oxidising environments have long been recognised to cause accelerated FCGR (da/dN) in air, especially under dwell conditions, as a result of intergranular crack growth [6-13]. However, during prolonged dwell periods, creep strain accumulation (due to time-dependent plasticity) can lead to stress relaxation effects in the vicinity of the crack-tip which have been seen to play a beneficial role in retarding intergranular crack growth mechanisms [17, 18]. Under extreme conditions (overload), time-dependent plasticity might develop to such extent that the crack can no longer advance by oxide cracking, thereby switching off the environmentally-enhanced crack growth mechanism during the dwell period [9, 22]. Note that at particular high temperatures (>750°C), creep damage processes characterised by intergranular micro-

void coalescence can start to dominate in both air and vacuum environments and may also lead to accelerated FCGR during dwell periods [4, 16]. Furthermore, microstructural changes arising during prolonged thermal exposures can also control plasticity responses [8]. In this current paper, the effects of oxidation and plasticity are decoupled to focus on local mechanical stress fields due to (time-dependent) plasticity alone. The rationale for performing stress-based FE modelling to investigate time-dependent plasticity is ascribed to the significance of stress modifications in the crack-tip region for characterising DFCG. The following discussion attempts to address how numerical models may draw some insight on dwell crack growth mechanisms (and controlling parameters).

4.1. Dwell effects

A comprehensive (time-dependent) constitutive creep model is utilised here to carry out stress-based FEA on a 2D cracked geometry. Computed stress-distance profiles (for example, in **Fig. 6**) show that the introduction of dwell periods can lead to local stress relaxation, which has experimentally been reported to beneficially influence DFCG behaviour either by reducing FCGR or even promoting crack arrest [7, 17, 18]. Predicted peak tensile stresses are 4775 and 4740 MPa for applied linear elastic stress intensity factors of 21.7 and 32.6 MPa.m$^{1/2}$ respectively at a time of one second. These are similar to those that can be calculated from an earlier (time-independent plasticity) analysis reported by McMeeking [32]. During dwell, the crack-tip region accumulates more creep strain which causes tensile stresses to further relax local peak stresses and their decay with distance from the crack-tip. It is also of note that crack-tip blunting is predicted to occur (**Fig. 7**). For example, over a 3600s dwell period, the CTOD is predicted to increase from 1.2 and 2.4 µm (upon initial loading) to 1.5 and 3.4 µm, for σ_{dwell} of 200 and 300 MPa respectively. Although these are relatively modest increases in CTOD in absolute terms, they are still considered to have potential to promote crack growth retardations, and such retardations are routinely seen experimentally at lower ranges of applied stress intensity factors [15, 16].

In light of the data simulations, creep micro-mechanisms operate in very local regions around the crack-tip. Dwell effects were shown to be lost in the far-field material and physical distances

governing the action of plasticity were predicted to lie within the micron-scale. A physically-based approach for characterising near crack-tip behaviour uses the CTOD parameter. Crack blunting (due to local creep deformation) affects a zone of a few CTOD ahead of the crack-tip. With longer hold (dwell) times, this 'damage zone' is pushed forward and the extent of the relaxed stress fields spreads. On the basis of time-dependent plasticity only (assuming no creep damage can occur in crack-tip regions), standard dwell simulations predict that the local crack-tip stress state becomes less damaging with increasing dwell time. Since crack-opening stress fields are decaying over time, driving forces for crack growth are lowered which potentially reduces FCGR and thus fracture becomes more and more unlikely. So, for example, if no crack growth is observed over a dwell cycle 1-300-1-1, then based purely on the stress relaxation (and a fracture criterion of maximum local stress) no crack growth is to be expected over a longer dwell cycle of, for example, 1-600-1-1. Note that some caution should be exercised if this approach is ever to be extended to components which can be subjected to significant net section stresses and where ("bulk") creep may occur.

However, high-temperature material degradation due to oxidation majorly contributes to crack growth (i.e. accelerated DFCGR) and will inevitably influence the potential for fracture (due to GB embrittlement and oxide breaking). So, the overall description for DFCG needs to account for oxide growth and its influence on local stress states. Detailed calculations [19] of oxide formation ahead of a crack-tip under stressed and stress-free conditions have shown that compressive stress states develop in the oxide. Compressive stresses gradually decrease and become tensile with further distance away from the crack-tip towards the front end of the oxide. These stress states then become significantly more important in magnitude as the oxide grows and thus failure will eventually occur. Here, the "paradox" is that local stress fields become less damaging (more relaxed) as dwell time increases but longer dwell times are more damaging because they are observed to result in increased crack growth rates (da/dN). Moreover, it is apparent that immediately at the beginning of dwell periods the oxide will be under the least compression when at its thinnest and local tensile stresses are at their highest (in the crack-tip region) because they have not yet relaxed as much. Hence, logic claims that fracture cannot be defined by a unique stress at a unique point since otherwise the oxide is predicted to break straightaway at the start of the dwell period. Clearly due to the complexity associated with the interactions of the time-

dependent mechanisms of oxide growth and time-dependent stress relaxation, a stress-based analysis on its own is insufficient to derive an absolutely precise fracture criterion.

4.2. Overload effects

The motivation to investigate overload cycling conditions comes from the need to more accurately model engine flight profiles in order to improve lifing strategies. Overload waveforms better represent in-service stress states; they describe partial unloading from maximum to dwell load which replicates the switch in engine capacity from "take-off" to "climb" events during typical flight cycles. Crack growth retardation phenomena have experimentally been observed to occur when partially unloading from higher stress conditions (overload) [9, 13, 18, 21-23]. For fatigue cycling, several mechanisms (crack blunting, branching, strain-hardening, crack-tip closure) have been proposed in an attempt to rationalise crack growth retardation. Despite some discrepancies, they all emphasise the importance of local crack-tip stress fields. For dwell cycling, the most relevant concept postulates that the preferential unloading of crack-tip stresses leads to significant changes in near-tip stress levels which introduce residual zones ahead of the crack-tip [21, 22].

In this current paper, FEA modelling of overload conditions has revealed two distinctive features with important implications on DFCG behaviour. Significant reductions in local tensile stresses induce a compressive (residual) stress zone just ahead of the crack-tip which effectively lowers crack driving forces. Secondly, large near-tip stress relaxation driven by active creep mechanisms occurs during subsequent dwell periods. Stress relaxation effects are associated with inelastic creep strain rates near the crack-tip which may delay intergranular damage processes. Altogether, this sensibly explains how overload cycling conditions may reduce FCGR or in some cases even promote crack arrest. This current paper specifically studies and compares the crack-tip stress field criterion under standard dwell and overload conditions. The beneficial effect of OL on (potential) crack growth retardation reduces over time as crack-opening stress fields recover back from their "unloaded" state. Therefore, it is natural to reason that there is an incubation time associated to each OL condition which defines the time it takes for local crack-tip stresses to converge back to identical stress states under both loading cases. The

incubation time characterises the extent of crack growth retardation and is here derived by applying an engineering approximation which relies on the basis of matching crack-tip stress relaxation curves computed for overload and dwell-only simulations within a 2% difference. A key differentiation between 'partial' and 'full' retardation is established as outlined below and correlates well to similar classifications presented in previous studies [9]:

(i) If $t_{inc} < t_{dwell}$: crack growth is inhibited whilst near-tip stresses are recovering towards their non-overload (dwell) level. Once local tensile stresses have fully relaxed back *at* $t_{inc} = t_{dwell}$ time-dependent crack growth will resume as usual for the remainder of the dwell period (resulting in partial retardation) and thereafter response to crack growth mechanisms is identical;

(ii) If $t_{inc} > t_{dwell}$: near-tip stresses will never relax back to their non-overload (dwell) level within one simulated cycle. Time-dependent components of crack growth are completely lost, and full retardation must be achieved back to fatigue baseline rates (which are controlled primarily by the stress intensity factor range).

A noteworthy finding of the presented modelling work is that the extension of overload dwell time (t_{OL}) from 1 to 10 seconds leads to a minimum six-fold increase in incubation time. The model suggests that 1s OL does not significantly affect local crack-opening stress states (compared against STD dwell) whereas 10s OL beneficially reduces near crack-tip stress levels which may even become compressive. For longer holds at OL, more extensive creep strain accumulates around the crack-tip which results in crack-tip stresses relaxing back more slowly as creep strain evolution approaches a steady state. FEA modelling predicts that a 240s incubation time associated with 1-10-1-300 delays time-dependent crack growth so that, instead of having the full dwell effect of 300s, only 60s of dwell are contributing. Yet, modelling results do not capture that even a short (1s) and small (5%) OL have been observed to reduce FCGR compared to those associated with dwell-only loading [9, 18].

The methodology of analysis used in the current paper relies on the selection of specific dwell times and particular nodes within the post-processing module of ABAQUS. This inevitably leads to a weakness in the calculation of incubation times which are performed at an individual point (here at the

first node 5 nm ahead of the crack-tip). Indeed, it has been shown that the peak in crack-opening stress distribution reduces and moves further ahead with time under standard dwell conditions **(Fig. 6)**, precise incubation times may differ slightly if local stresses are interrogated at other nodes further ahead of the crack-tip. Thus, the model as presented here captures the mechanics of the crack-tip stress field (in the absence of any oxide present) accurately at the point interrogated. In addition, the influence of oxide growth on local stress states has not been considered and so it is difficult to determine an absolute value for a fracture stress criterion from this modelling work alone. This paper has however demonstrated the importance of local stresses around the crack-tip when relating overload effects and time-dependent plasticity.

As many mechanisms compete and combine to influence DFCG behaviour, it is important to highlight that the complete story of overload effects should be concerned with whether intergranular cracking occurs during overload hold (at σ_{OL}) due to time-dependent oxide formation and subsequent embrittlement of the GB. Even if local tensile stresses take longer to recover when extended OL periods (such as 10s) are applied, potential retardation could be overly optimistic if crack growth can occur during the OL dwell period (such as 10s) itself.

In regards to component integrity assessments, the mechanisms involved during OL cycling and associated retardation phenomena still require a comprehensive and complete description. The extent of large reductions in FCGR has important implications on lifing strategies. Based on the importance of crack-tip stresses and time-dependent plasticity, computational techniques as presented in this paper have allowed insight into how overloads can lead to significant retardation effects. Current lifing approaches are still extremely conservative and understanding aided by numerical modelling has potential to extend certified life in aero-engine turbine discs.

5. Conclusions

A detailed numerical creep model based on microstructural variables has successfully been implemented. Numerical outputs from the FE model, considering time-dependent plasticity and subjected to standard dwell and overload cycles, represent the basis for performing a stress-based

analysis of the development of mechanical fields ahead of the crack-tip. The main conclusions are summarised as follows.

1. FEA modelling has provided insight into DFCG behaviour by considering effects of time-dependent plasticity. Here, it particularly adds confidence to the underlying mechanism of stress relaxation arising from such time-dependent plasticity and illustrates how rapidly local crack-tip stresses can relax.
2. The local refined mesh has been validated against the rationale of physical distances (micro-scale) involved in controlling the action of time-dependent processes. FEA results considered after initial loading (at a time of one second) have also shown good correlation with previous (time-independent) plasticity analysis in terms of both the value and location of local peak stress values.
3. Introduction of dwell periods leads to near-tip stress relaxation by time-dependent plasticity. With increasing hold times, a larger zone ahead of the crack-tip is affected by crack-tip blunting and the extent of relaxed stress fields is pushed forward due to creep strain accumulation.
4. The beneficial characteristics of overloads are reasonably well captured. FE simulations are able to identify (i) the compressive stress fields which lower crack driving forces and (ii) the large near-tip stress relaxation. A numerically-derived incubation time has successfully been applied in predicting the general trends of achieving more pronounced retardation effects with larger overload factors and extended overload dwell. FEA modelling predicts a significant difference in behaviour between a 1s and 10s overload period.
5. Modelling work has given insight into the existing competition between oxide growth and plasticity. The importance of studying local crack-tip stress fields in regards to DFCG has been emphasised. It is plausible to conclude that the main characteristics for applications to lifing could be captured on the basis of crack-tip stresses by plasticity only. A precise definition of a physically-based fracture criterion for oxide failure under dwell loading still remains a future challenge**.**

Acknowledgments

The authors are grateful for the support of this work by Rolls-Royce. The present work was carried out at the Rolls-Royce University Technology Center at the University of Birmingham in the framework of a final year (master's) project.

References

1. Hardy MC, Zirbel B, Shen G, Shankar R. Developping damage tolerance and creep resistance in a high strength nickel alloy for disc applications. *TMS: Superalloys 2004*. 2004:83-90.
2. Reed RC. *The superalloys: fundamentals and applications*: Cambridge University Press; 2006.
3. Knowles DM, Skelton DK. High temperature fatigue of a polycrystalline nickel base superalloy. *Materials Science and Technology*. 2001;17(11):1403-1412.
4. Knowles DM, Hunt DW. The influence of microstructure and environment on the crack growth behavior of powder metallurgy nickel superalloy RR1000. *Metallurgical and Materials Transactions*. 2002;A33:3165-3172.
5. Pineau A, Antolovich SD. High temperature fatigue of nickel-base superalloys - A review with special emphasis on deformation modes and oxidation. *Engineering Failure Analysis*. 2009;16:2668-2697.
6. Yu SY, Li HY, Hardy MC, McDonald SA, Bowen P. Mechanisms of dwell fatigue crack growth in an advanced nickel disc alloy RR1000. *MATEC Web of Conferences*. 2014;14.
7. Liu X, Kang B, Chang KM. The effect of hold-time on fatigue crack growth behaviors of WASPALOY alloy at elevated temperature. *Materials Science and Engineering*. 2003;A340:8-14.
8. Turan D, Hunt D, Knowles DM. Dwell time effect on fatigue crack growth of RR1000 superalloy. *Materials Science and Technology*. 2007;23(2):183-188.
9. Fisk JC. Effects of creep and oxidation interaction on high temperature crack growth behaviour of nickel based superalloys: University of Birmingham; 2013.

10. Pang HT, Hardy MC, Hide N, Wilcock IM, Henderson MB, Reed P. Comparison of fatigue crack propagation in nicel base superalloys RR1000 and Udimet 720Li. *Materials Science and Technology*. 2016;32(1):22-39.

11. Ghonem H, Nicholas T, Pineau A. Elevated temperature fatigue crack growth in alloy 718 - Part II: Effects of environmental and material variables. *Fatigue and Fracture of Engineering Materials and Structures*. 1993;16(6):557-590.

12. Onofrio G, Osinkolu GA, Marchionni M. Fatigue crack growth of UDIMET 720 Li superalloy at elevated temperature. *International Journal of Fatigue*. 2001;23:887-895.

13. Gustafsson D, Lundström E. High temperature fatigue crack growth behaviour of Inconel 718 under hold time and overload conditions. *International Journal of Fatigue*. 2013;48:178-186.

14. Evans HE, Li HY, Bowen P. A mechanism for stress-aided grain boundary oxidation ahead of cracks. *Scripta Materialia*. 2013;69:179-182.

15. Kitaguchi HS, Li HY, Evans HE, Ding RG, Jones IP, Baxter G, et al. Oxidation ahead of a crack tip in an advanced Ni-based superalloy. *Acta Materialia*. 2013;61:1968-1981.

16. Li HY, Sun JF, Hardy MC, Evans HE, Williams SJ, Doel TJA, et al. Effects of microstructure on high temperature dwell fatigue crack growth in a coarse grain PM nickel based superalloy. *Acta Materialia*. 2015;90:355-369.

17. Telesman J, Gabb TP, Ghosn LJ. Separating the Influence of Environment from Stress Relaxation Effects on Dwell Fatigue Crack Growth in a Nickel-Base Disk Alloy. 13th International Symposium on Superalloys; Seven Springs (United States): Minerals, Metals and Materials Society; 2016.

18. Telesman J, Gabb TP, Ghosn LJ. A novel methodolody for modeling dwell fatigue crack growth in Ni-based superalloys. *International Journal of Fatigue*. 2020;133.

19. Fang CZ, Basoalto HC, Anderson MJ, Li HY, Williams S, Bowen P. A numerical study of the influence of grain boundary oxides on dwell fatigue crack growth of a nickel-based superalloy. *Journal of Materials and Technology*. 2021;104, 30 March 2022: 224-235 (published online 08/09/2021).

20. Molins R, Hochstetter G, Chassaigne JC, Andrieu E. Oxidation effects on the fatigue crack growth behaviour of alloy 718 at high temperature. *Acta Materialia*. 1997;45(2):663-674.

21. Ponnelle S, Brethes B, Pineau A. High temperature fatigue crack growth rate in Inconel 718: Dwell effect annihilations. *European Structural Integrity Society*. 2002;29:257-266.

22. Telesman J, Gabb TP, Kantzos P, editors. Effect of overloads on time dependent fatigue crack growth in a nickel based superalloy. *International Fatigue Congress* 2002; Stockholm (Sweden).

23. Saarimäki J, Moverare J, Eriksson R, Johansson S. Influence of overloads on dwell time fatigue crack growth in Inconel 718. *Materials Science and Engineering*. 2014;A612:398-405.

24. Reed RC, CMF R. 22.5.4. Model for composition dependence of creep deformation. Physical Metallurgy: 22 - Physical Metallurgy of the Nickel-Based Superalloys: Elsevier; 2014. p. 2215-2290.

25. Orowan E. The Creep of Metals. *Journal West of Scotland Iron and Steel* 1946-1947;54:45-96.

26. Dyson BF. Microstructure based creep constitutive model for precipitation strengthened alloys: theory and application. *Materials Science and Technology*. 2009;25(2):213-220.

27. Basoalto HC, Sondhi SK, Dyson BF, McLean M. A generic microstructure explicit model of creep in nickel-base superalloys. *TMS: Superalloys 2004*. 2004:897-906.

28. Basoalto HC, Brooks JW, Di Martino I. Multiscale microstructure modelling for nickel based superalloys. *Materials Science and Technology*. 2009;25(2):221-227.

29. Coakley J, Dye D, Basoalto H. Creep and creep modelling of a multimodal nickel-base superalloy. *Acta Materialia*. 2011;59(3):854-863.

30. ABAQUS, Version 6.13 User's manual, SIMULIA, Providence, RI, 2013 [Internet]. Simulia.

31. Standard Method of Test for Plane-Strain Fracture Toughness of Metallic Materials (Designation: E 399-72), *Annual Book of ASTM Standards, 1972,* Part 31, pp. 955-974.

32. McMeeking RM. Finite deformation analysis of crack-tip opening in elastic-plastic materials and implications for fracture. *Journal of Mechanical Physical Solids*. 1977;25:357-381.

Figure Legends

Fig. 1: Three typical examples of engine loading cycles: baseline cycling, dwell cycling, and overload cycling.

Fig. 2: Crack growth resistance curves (da/dN vs ΔK_{full}) showing an example of dwell and overload-dwell effects on DFCG behaviour in LSHR alloy at 704°C [18].

Fig. 3: Schematic illustration showing the variation in normal out-of-plane stress along oxide intrusion ($0 \leq x \leq l$) in the absence of an applied load [14].

Fig. 4: Schematic of the boundary conditions applied to the 2D SENT specimen geometry. Illustration of the implemented 2D FE mesh in ABAQUS. Global mesh with coarse mesh and a locally refined mesh near the crack-tip [19].

Fig. 5: Simulated loading waveforms **(a)** The standard dwell cycle is modelled as 1-t_{dwell} stress waveform: initial stress ramp-up to σ_{dwell} in 1s (t_1) and hold at σ_{dwell} for t_{dwell}. **(b)** The overload cycle is modelled as 1-t_{OL}-1-t_{dwell} stress waveform: initial stress ramp-up to σ_{OL} in 1s (t_1), hold at overload until t_2 (t_2 - t_1 denotes the overload dwell time), unload from σ_{OL} to σ_{dwell} in 1s (t_3) and normal hold at σ_{dwell} for t_{dwell}.

Fig. 6: Stress-distance profiles at different points for the FE model (RR1000 at 650°C) subjected to simulated dwell-only cycles with σ_{dwell} of 300 MPa. Stress distribution plotted in regards to crack-tip opening stress S22 and S22 normalised by the yield stress (σ_y = 1000 MPa).

Fig. 7: Crack-tip opening displacement plotted versus time, with CTOD/2 numerically investigated at the CTO-node selected (2 μm behind the crack-tip).

Fig. 8: Stress-distance profiles at different time points (dwell times) for FE model subjected to σ_{dwell} = 300 MPa, OLF = 1.05 and t_{OL} = 10s.

Fig. 9: Local stress-distance profiles compared for standard dwell, 1s and 10s overload condition (σ_{dwell} = 300 MPa and OLF = 1.05) (a) t_{dwell} = 30s, (b) t_{dwell} = 120s, (c) t_{dwell} = 300s.

Fig. 10: Crack-tip stress-time histories (σ_{22} versus non-overload dwell time) are generated at the first node ahead of the modelled crack-tip and compare four different overload conditions with the standard (STD) dwell loading case (for σ_{dwell} = 300 MPa).

Declaration of interests

☒The authors declare that they have no known competing financial interests or personal relationships that could have appeared to influence the work reported in this paper.

☐The authors declare the following financial interests/personal relationships which may be considered as potential competing interests:

Modelling and predictions of time-dependent local stress distributions around cracks under dwell loading in a nickel-based superalloy at high temperatures

Florence M. Muller [a,1,*]

Chizhou Fang [b,*], Hector C. Basoalto [b], Steve Williams [c], Paul Bowen [a]

[a] School of Metallurgy and Materials, University of Birmingham, Edgbaston, Birmingham B15 2TT, United Kingdom

[b] Department of Materials Science and Engineering, University of Sheffield, Mappin St, Sheffield S1 3JD, United Kingdom

[c] Institute of Structural Materials, Swansea University, Swansea SA1 8EN, United Kingdom

* Corresponding authors:

Florence M. Muller

FlorenceMarie.Muller@ugent.be

Chizhou Fang

c.fang@sheffield.ac.uk

[1] Medical Image and Signal Processing (MEDISIP, ELIS, IBiTech), Faculty of Engineering and Architecture, Campus Ghent University Hospital (Entrance 36), Corneel Heymanslaan, Gent 9000, Belgium (present affiliation)

Abstract

Finite element (FE) analysis modelling of crack configurations was used to provide insights into the role of time-dependent deformation on dwell fatigue crack growth (DFCG) in turbine disc alloys. In particular, the potential influence of time-dependent deformation on fatigue crack growth rates observed during dwell holding periods and the potential crack growth retardation phenomena that can occur for overload-dwell cycles were investigated. The FE model evaluated the mechanical stress state evolution in a two-dimensional cracked geometry subjected to standard dwell and overload-dwell stress waveforms for a given microstructural condition (based on its γ' particle distribution). Crack-opening stress distributions as a function of dwell time and distance ahead of the crack-tip were interrogated, with the aim to investigate the potential influence of local crack-tip stresses on crack growth during dwell holding periods and the potential for crack growth retardation following overload cycles. Stress distribution profiles predicted by dwell-only simulations showed how quickly local crack-tip stresses relax due to time-dependent plasticity. Characteristic effects of overloads of dwell crack growth resistance observed in experiments were also reasonably well captured. A numerically-derived incubation time was successfully applied in predicting the general trends of achieving more pronounced retardation effects with larger overload factors and extended periods of overloading prior to periods of dwell. FE modelling predicted a significant difference in behaviour between an overload for a given overload factor with a hold time at peak load of 1s and 10s. This study emphasises the importance of studying local crack-tip stresses in regards to characterising DFCG behaviour of turbine disc alloys.

Keywords

Dwell fatigue crack growth, Finite element modelling, Nickel-based turbine disc alloys, Overload, Time-dependent plasticity

1. Introduction

Gas turbine development drives to optimise engine performance and efficiency by pushing new generation disc alloys (powder metallurgy nickel-based superalloys) to increasing levels of operating temperature regimes [1, 2]. At high temperatures (>500°C) in air, a mechanism of brittle intergranular dwell fatigue crack growth (DFCG) is observed and has been discussed as being influenced by several interacting and (often) competing contributions of: (i) cyclic plastic deformation; (ii) time (and stress)-dependent oxide formation and/or oxygen embrittlement of grain-boundaries (GB); and (iii) time-dependent plasticity (creep deformation) [3-6]. Such brittle intergranular fracture occurs in air, but not in vacuum. At the highest temperatures (typically above 750°C) the intergranular crack growth mechanism transitions to creep fracture by intergranular micro-void coalescence, which can now occur in both air and in vacuum. Since such brittle intergranular mechanisms in loading cycles with long dwell periods can give crack growth rates (CGR) that are markedly higher than those observed for transgranular crack growth in fast loading cycles, DFCG in Ni-based superalloys has potential to become one limiting factor on a declaration of certified life for turbine disc applications. **Fig. 1** illustrates three loading waveforms commonly used to simulate representative engine loading cycles.

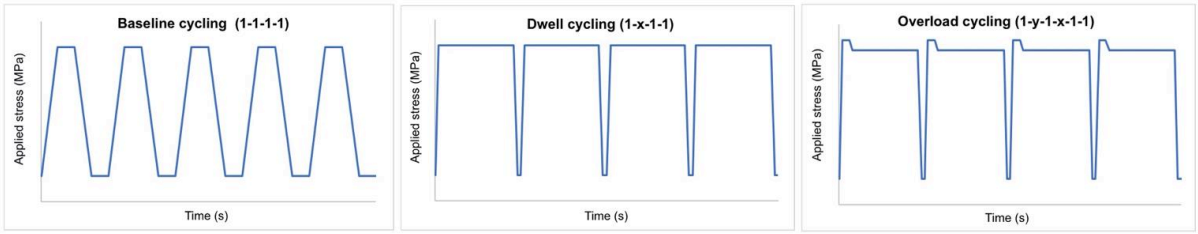

Fig. 1: Three examples of typical engine loading cycles: baseline cycling, dwell cycling and overload cycling.

Oxidising environments have long been recognised to cause significant increases FCGR per cycle, especially when introducing dwell periods at peak load, as a result of intergranular crack growth (**Fig. 2**) [7-10]. Intergranular failure modes and accelerated FCGR are primarily controlled by oxygen/oxide damage effects at and/or very close to the growing crack-tip [6, 11-13]. Stress-assisted

grain-boundary oxidation (SAGBO) is widely accepted as the dominant mechanism accounting for the detrimental influence of oxygen on DFCG behaviour [14-16]. Under combined conditions of high stress and temperature, the preferential (and accelerated) formation and growth of an oxide intrusion along a GB ahead of the crack-tip results in GB fracture, thereby increasing CGR with oxide failure. When crack growth tests are repeated in vacuum, dwell effects are almost completely eliminated [3, 9, 10, 12], unless the temperature is high enough (>750°C) for creep crack growth processes (intergranular micro-void coalescence) to be activated [16, 17].

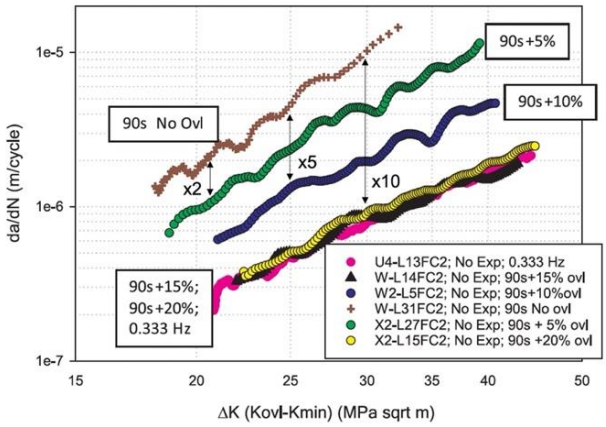

Fig. 2: Crack growth resistance curves (da/dN vs ΔK_{full}) showing an example of dwell and overload-dwell effects on DFCG behaviour in LSHR alloy at 704°C [18].

Much previous research has focused on studying the relative significance of creep damage and environmental degradation on crack-tip damage. However, a full description of DFCG behaviour needs to account for stress relaxation effects occurring in the vicinity of the crack-tip, particularly during prolonged dwell periods. Stress relaxation will reduce elevated tensile stresses local to the crack-tip. If a stress-controlled fracture criterion is invoked for oxide (or embrittled GB) cracking, then this relaxation (due to time-dependent (creep) deformation) might have the potential to retard intergranular crack growth. A complete analysis of any oxide cracking mechanism will also consider potential effects of the oxide putting itself into compression as it grows (due to a volumetric expansion upon formation) as shown schematically in **Fig. 3** [14, 19]. In this current paper, emphasis is put on understanding and predicting time-dependent plasticity which will promote near-tip stress relaxation (due to the

accumulation of creep strain) and concomitant crack-tip blunting which may have the potential to reduce the rate of oxide cracking [17, 18]. Given the opposing effects over time (within any dwell period) of environmental degradation (increased oxide growth and/or GB embrittlement expected to accelerate DFCGR) and near-tip stress relaxation (which may decrease DFCGR) [6, 16, 20] it is useful to decouple the effects of creep deformation and oxidation to provide further insight on the separate action of these local mechanisms. So, this current paper considers stress relaxation effects arising from time-dependent plasticity only.

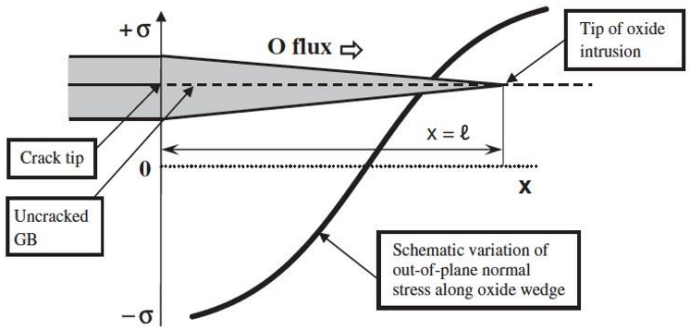

Fig. 3: Schematic illustration showing the variation in normal out-of-plane stress along oxide intrusion ($0 \leq x \leq l$) in the absence of an applied load [14].

The introduction of an overload segment prior to dwell periods may result in further significant reductions of FCGR compared to (otherwise similar) dwell-only cycling, with overload effects usually being interpreted in terms of transient changes to local crack-tip plasticity. However, within this field, relatively few studies have been reported in the scientific literature [9, 13, 18, 21-23]. For severe overload conditions, it has been observed that damaging dwell effects can be eliminated entirely, with growth rates decreasing down to levels of baseline loading (fatigue crack growth) (**Fig. 2**) after [18]. These dramatic effects of suppressed or retarded crack growth have been rationalised by significant variations in near-tip stress relaxation response [21, 22]. Stress relaxation at the crack tip will be beneficial provided that the influence from lower stresses and crack tip blunting is greater than any potential debit from accumulating higher levels of creep strain. The complexity of this crack growth retardation reinforces the motivation here to analyse effects of time-dependent plasticity alone.

The need for more detailed physical insight on DFCG behaviour of turbine disc alloys has driven the application of FEA modelling of crack configurations. Both a comprehensive mesh formulation and a detailed numerical creep model (based on microstructural variables) were available from previous work by some of the current authors [19]. The model here considers constitutive equations for material creep and plasticity alone (while the original model also includes effects of oxidation and oxide growth). By decoupling the effects of oxidation and plasticity, this modelling work focuses on the underlying mechanism of stress relaxation due to time-dependent plasticity and studies crack-opening stress modifications in the vicinity of the crack-tip to characterise DFCG behaviour of Ni-based superalloys. This paper describes the FE method used to evaluate the mechanical stress state evolution in a 2D cracked geometry subjected to standard dwell and overload stress waveforms for a given microstructural condition (γ' particle distributions) somewhat typical of the distributions applicable to the proprietary alloy RR1000. The primary purpose of this paper is to investigate the potential influence of local crack-tip stresses on crack growth during dwell holding periods and the potential for crack growth retardation following overload cycles. It is limited here to a time-dependent stress field analysis of a stationary crack and it does not incorporate any node release schemes to simulate crack advance.

2. Materials and Methods

2.1. Numerical implementations

2.1.1. *The Finite Element model*

The geometry of the FE model used in this study, a 10x10 mm^2 cross-sectional area representative of the single-edge notched tension (SENT) specimen geometry, is shown in **Fig. 4** . The use of plane-strain elements is consistent with a knowledge that the individual crack growth mechanism to which the current FE model outputs will be applied occurs more readily away from plane stress regions. For computation efficiency, the global model includes a coarse mesh away from the crack and a fine mesh of 25 nm size elements near the crack-tip which is needed to obtain accurate stress states locally. The

justification for using such a refined local mesh is rationalized in view of the scale of the envisaged crack growth increments and is discussed later.

The boundary conditions are also shown in **Fig. 4**. AB represents a 2 mm stationary crack. BC denotes the GB ahead of the crack-tip defined by a symmetry boundary condition in order to account for the material contact that prevents vertical displacement. Point B represents the crack-tip and point C is restrained. The applied stress acts on the top surface ED which is allowed to deform freely under this pressure loading.

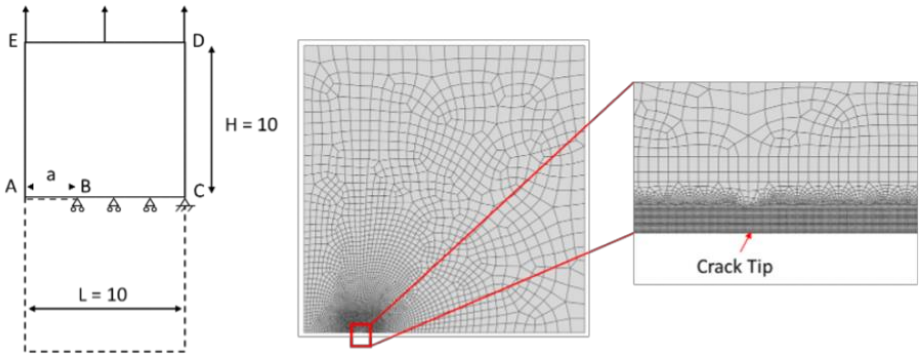

Fig. 4: Schematic of the boundary conditions applied to the 2D SENT specimen geometry. Illustration of the implemented 2D FE mesh in ABAQUS. Global mesh with coarse mesh and a locally refined mesh near the crack-tip.

2.1.2. *The Finite Element mesh*

The FE mesh used here is constructed using a local refined mesh near the crack-tip (with element size of 25 nm) and a coarser mesh away from the crack-tip, as shown in **Fig. 4**. The necessity for a refined mesh locally can be justified in terms of the local mechanisms envisaged. That the physical length scales actually involved here are on an action zone very local to the crack-tip as can be appreciated both in terms of crack growth per dwell cycle where: for one-hour dwell testing at 650°C in air, FCGR in RR1000 are found experimentally to be around 0.03-0.04 mm/cycle which is roughly equivalent to 8-11 nm/s for values of K (ΔK) of 20-30 MPa.m1/2 [9]; and in terms of oxide growth: ahead of stationary cracks, where oxides can grow to about 4.5 µm when exposed under a constant load (stress intensity factor) for 5hrs [15] (which can be estimated on a linear basis with time to be 15 nm/s).

2.1.3. *Material model and microstructure*

The high-temperature strength of Ni-based superalloys (of a given grain size) is primarily derived from the distribution of strengthening γ' particles which disrupt continuous glide of dislocations. Pinned dislocations overcome γ' particles through local climb and creep can be treated as a jerky glide process, with climb and glide events happening simultaneously [24, 25]. The mechanical creep behaviour is therefore most suitably represented by a constitutive model that connects microstructure and macroscopic creep rate. Dyson [26] derived a microstructure-explicit state variable approach for uni-modal precipitate-strengthened alloys. Basoalto *et al.* [27-29] extended the dispersion-controlled creep model developed by Dyson [26] to account for multi-modal γ' distributions. For this type of extended creep model, the constitutive equations are explicitly expressed in terms of quantitative measures of initial microstructural features and their subsequent rates of evolution. Details can be found elsewhere [19] but it is noted that the model parameters have been optimised by extensive correlations with experimental data and the output of such correlations are reproduced in **Table 1**.

The microstructure-explicit visco-plastic model established by Basoalto has been adopted in the present modelling work to describe the mechanical material behaviour of a standard heat-treated microstructure typical of that to be found in fine-grained RR1000. The commercial FE software ABAQUS is used for performing non-linear static stress analyses. Constitutive laws are implemented and numerically solved in an ABAQUS user-defined subroutine (UMAT) [19, 30] . In this study, spatial-temporal evolution of the multi-modal γ' size distribution is not considered. The associated microstructural model input are the γ' dispersion parameters, i.e. volume fraction and mean size of primary, secondary and tertiary γ'. Creep rates scale with volume fraction of γ' precipitates and there is non-linear scaling with inter-particle distances (which means the higher the number density of particles, the smaller the spacing and hence the lower the creep rates). Controlling the creep rates with particle dispersion is essential for controlling the stress relaxation ahead of the crack-tip which in turn influences DFCG behaviour. Grain size distribution effects are neglected based on the assumption that creep deformation is controlled by interparticle distances and not grain dimensions. Since this creep model

194 does not contain any dependency on grain size, it is applicable to situations around crack-tips where
195 local stresses are high, and deformation will be dominated by dislocation activity alone This, however,
196 implies that any hardening behaviour of flow stresses (Hall-Petch type) will not be captured. The γ'
197 particle distributions considered in the present paper are given in **Table 2**. They are representative of
198 distributions that may occur in fine-grained variants of the RR1000 alloy.
199
200 **Table 1:** Microstructural model parameters used in the constitutive model [19, 27].

Burger vector, b (m)	2.54×10^{-10}
Taylor factor, M	3.1
Dislocation multiplication parameter, C	100
Activation energy, Q (kJ.mol^{-1})	305
Pre-exponential diffusivity, D_0 (m^2.s^{-1})	1×10^{-5}
Jog density, c_j	1
Mobile dislocation density, ρ_m (m^{-2})	10^{10}
Misfit stress (MPa)	-120
Young's Modulus (GPa)	188
Poison's ratio	0.33

201
202 **Table 2:** Volume fraction and average diameter size of primary, secondary and tertiary γ' for a simulated
203 (fine-grained) RR1000 microstructure.

Primary γ'	Volume fraction, V_{f1}	12 %
Secondary γ'	Volume fraction, V_{f2}	28 %
	Average size, $\emptyset_2$	120 nm
Tertiary γ'	Volume fraction, V_{f3}	5 %
	Average size, $\emptyset_3$	20 nm
Total volume fraction of γ'		45 %

204
205 2.1.4. *Loading waveforms and simulated conditions*
206 Within the scope of this project, the simulations explore the mechanical stress fields near a stationary
207 crack-tip as a function of time-dependent plasticity. For a stationary 2 mm crack, applied far-field
208 stresses of 200 and 300 MPa give linear elastic stress intensity factors of 21.7 and 32.6 MPa.m$^{1/2}$

209 respectively using Equ.(1) where the "compliance" *C* for a SENT specimen is given as a function of
210 a/W [31] in Equ.(2).
211
212 $$K_I = C\,\sigma\,(\pi a)^{1/2} \quad (1)$$
213
214 $$C = 1.12 - 0.231\left(\frac{a}{W}\right) + 10.55\left(\frac{a}{W}\right)^2 - 21.72\left(\frac{a}{W}\right)^3 + 30.39\left(\frac{a}{W}\right)^4 \quad (2)$$
215
216 Dwell and overload loading waveforms are programmed as stress-time histories (but are guided in all
217 cases by previous experiments and/or envisaged by potential in-service loading). Appropriate time step
218 resolution definitions allow the time history to be split into smaller suitable time increments in order to
219 evaluate the stress state at each node at determined moments in time. The model is run under plane-
220 strain and isothermal conditions. Each condition is modelled by applying a single stress cycle,
221 neglecting the influence of any previous loading history and the simulation stops at the point of
222 unloading from dwell to minimum stress. The dwell-only waveform (1-t_{dwell}) is implemented by two
223 separate loading segments (**Fig. 5(a)**). The overload dwell waveform (1- t_{OL} -1- t_{dwell}) is defined by four
224 loading segments (**Fig. 5(b)**). To replicate the variation in stress with time during an overload, an
225 amplitude curve based on tabular data is implemented. The magnitude of overload is defined by an
226 overload factor (OLF) as follows, $\sigma_{OL}/\sigma_{dwell}$. Note that for OLF = 1.0 no overload is applied, and the
227 cycle reduces to the dwell-only waveform. The influence of nominal dwell stress (σ_{dwell}), dwell time
228 (t_{dwell}), overload factor (OLF) and overload hold time (t_{OL}) are studied. Loading waveforms are
229 simulated for subsequent dwell periods of 30, 120, 300, 600, 1200 and 3600 seconds. Overload factors
230 of 1.05 and 1.15, and overload hold times of 1 and 10 seconds are considered in this paper.
231

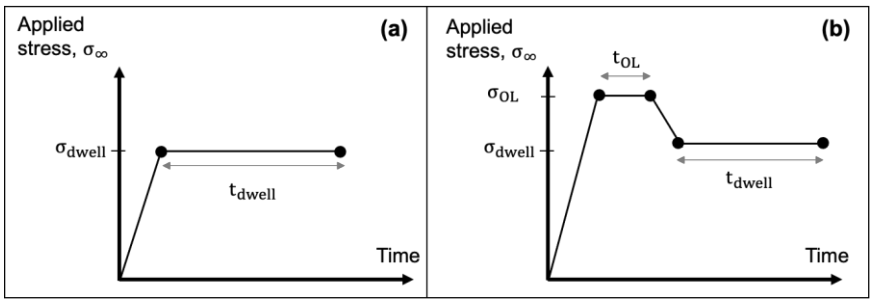

Fig. 5: Simulated loading waveforms **(a)** Standard dwell cycle is modelled as 1-t_{dwell} stress waveform: initial stress ramp-up to σ_{dwell} in 1s (t_1) and hold at σ_{dwell} for t_{dwell}. **(b)** Overload cycle is modelled as 1-t_{OL}-1-t_{dwell} stress waveform: initial stress ramp-up to σ_{OL} in 1s (t_1), hold at overload until t_2 (t_2 - t_1 denotes the overload dwell time), unload from σ_{OL} to σ_{dwell} in 1s (t_3) and normal hold at σ_{dwell} for t_{dwell}.

2.2. Data analysis

In the current paper, a stress-based approach was adopted to investigate crack-opening stress (σ_{22}) distributions as a function of dwell time and distance ahead of the crack-tip. The analysis specifically focused on local crack-tip stress fields and how these evolved during dwell (hold) periods when subjected to a standard dwell condition (STD) compared to an overload condition (OL). To generate spatial stress profiles, stress data was extracted from the local nodes and elements that, ahead of the modelled crack-tip, defined the plane containing the crack. One readily understood physically based approach for characterising near crack-tip behaviour uses the crack-tip opening displacement (CTOD) parameter. A sharp crack blunts initially on loading [32] and then it may also potentially blunt further under dwell (over time) with an external (far-field) load applied to the geometry. Thus, specifically for dwell-only simulations, the variation in CTOD as a function of time was investigated. To do this, a crack-tip opening node (CTO-node) was chosen 2 μm behind the crack-tip and examined in terms of its spatial vertical displacement. Note that this node was selected since it is close to the blunted crack-tip, yet one of the first nodes which will only suffer vertical displacement with further opening.

To consider a quantitative assessment of the effect of overloads on crack-opening stress fields, an engineering approximation was introduced to derive an incubation time which can be related to the potential for crack growth retardation following overload cycles, and which then leads to an effective dwell time (applied dwell time minus incubation time). Numerical outputs of σ_{22} with dwell time after

overloading were interrogated at the very first node (5 nm) ahead of the crack-tip and compared against the local stresses due to (non-overload) dwell times alone. This emphasises the importance of a local crack-tip stress criterion, but outputs of local stress profiles with time at a distance of up to 120 μm ahead of the crack-tip are also presented for selected cases.

3. Results: Application of the model

3.1. Standard dwell simulations

Stress-distance profiles predicted by the constitutive creep model using the multi-modal γ' microstructure listed in **Table 2** have been computed for dwell-only (standard) loading waveforms at 650°C. **Fig. 6** compares the crack-tip opening stress (S22) distribution at six different dwell times ranging from 30 to 3600 seconds for σ_{dwell} of 300 MPa. The stress-distance profile presented in **Fig. 6** is also shown with S22 normalised by the yield stress (S22/σ_y). Based on [19], the predicted average yield stress of the material (RR1000) is approximately 1000 MPa. During initial loading, the model predicts plasticity to occur close to the crack-tip, whereby the stress relaxes to approximately 3700 MPa at the crack-tip. When σ_{dwell} is first reached at t = 1s (during initial loading), dwell effects are not yet considered. Stress-distance curves demonstrate an overall reduction in σ_{22} with longer hold times, especially in the vicinity of the crack-tip. Significant stress relaxation notably arises within just a few tens of seconds into the dwell. However, beyond a certain distance away (0.07 mm for σ_{dwell} = 200 MPa; 0.18 mm for σ_{dwell} = 300 MPa) from the crack-tip, all profiles collapse into a single curve and re-join the t = 1s (initial loading) curve. General trends suggest that major changes to time-dependent plasticity occur in local regions very close to the crack-tip (typically within 20 μm).

Crack-opening stress distributions feature a local peak at a short distance away from the crack-tip. The magnitude of this maximum σ_{22} is predicted both to decrease and to move further ahead of the crack-tip with increasing hold (dwell) times (**Table 3**). The distance is expressed here as the distance over which tensile stress levels exceed 95% of this peak. With longer dwell times (and higher applied K levels), local tensile stresses within 95% of the peak stress extend over a larger distance from the

crack-tip. Similar to the original time-independent plasticity analysis of McMeeking [32], the magnitude of the maximum σ_{22} does not vary significantly with different values of applied K.

Fig. 7 shows the variation in CTOD as a function of time. Note that the computed values of CTOD denote only half of the actual CTOD because of modelling geometry symmetry. The initially very sharp crack blunts, with CTOD values for initial loading (at t = 1s) of 0.6 and 1.2 μm (for a σ_{dwell} of 200 and 300 MPa respectively). This CTOD value then increases further and appears to be levelling out to 0.74 and 1.68 μm over the subsequent one-hour dwell period (for σ_{dwell} of 200 and 300 MPa).

Table 3: Tabular data of maximum crack-opening stress (σ_{22}) and corresponding distance covering 95% of this peak ($d_{95\%}$). Results are presented for initial loading (at t = 1s) and different dwell times with σ_{dwell} = 200 and 300 MPa.

		Initial loading (t = 1s)					
Applied dwell stress σ_{dwell} (MPa)		200			300		
Maximum σ_{22} (MPa)		4775			4740		
		Dwell time (s)					
		30	120	300	600	1200	3600
200 MPa (21.7 MPa.m$^{1/2}$)	Maximum σ_{22} (MPa)	3340	3060	2895	2780	2670	2490
	$d_{95\%}$ (μm)	2.6	3.5	4.5	4.9	5.3	7.3
300 MPa (32.6 MPa.m$^{1/2}$)	Maximum σ_{22} (MPa)	3360	3020	2865	2750	2635	2460
	$d_{95\%}$ (μm)	4.5	9.2	10.3	11.6	13.3	15.2

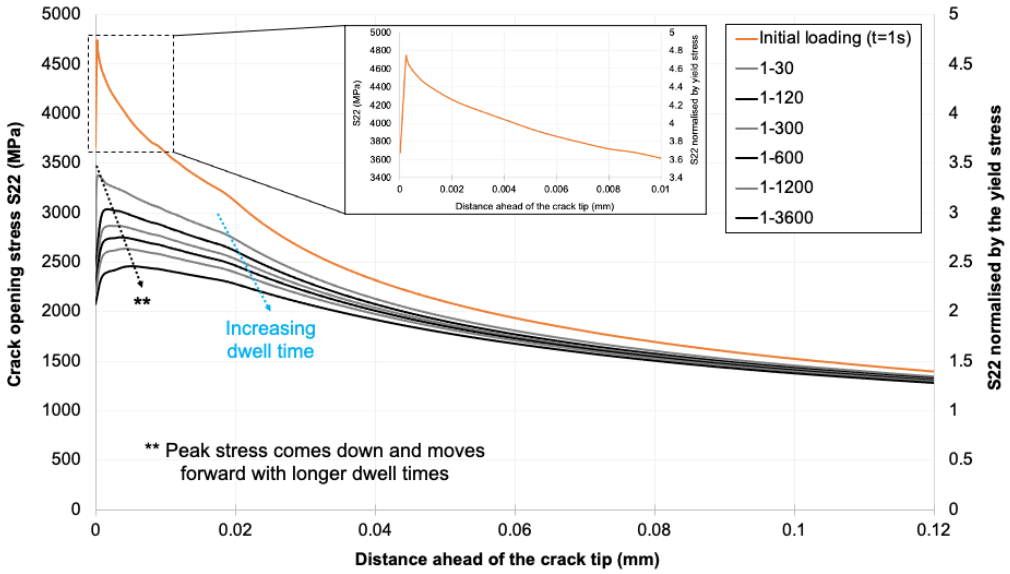

294

295 **Fig. 6:** Stress-distance profiles at different points for the FE model (RR1000 at 650°C) subjected to
296 simulated dwell-only cycles with σ_{dwell} of 300 MPa. Stress distribution plotted in regards to crack-tip
297 opening stress S22 and S22 normalised by the yield stress (σ_y = 1000 MPa).

298

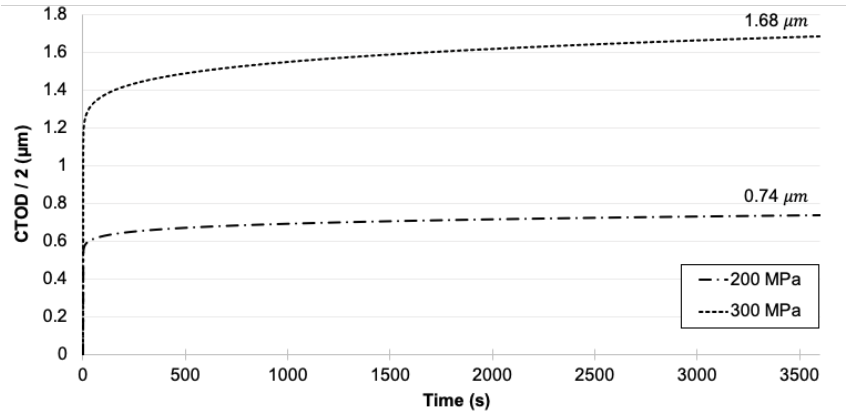

299

300 **Fig. 7:** Crack-tip opening displacement plotted versus time, with CTOD/2 numerically investigated at
301 the CTO-node selected (2 μm behind the crack-tip).

302

303 ## 3.2. Overload simulations

304 Four combinations of overload factors and overload dwell times (**Table 4**) were applied to the FE
305 model. Each simulation was conducted at 650°C with σ_{dwell} of 200 and 300 MPa, matching K values of
306 21.7 and 32.6 MPa.m$^{1/2}$ respectively.

307

Table 4: Overview of the four simulated overload conditions varying in applied overload factor (OLF) and overload dwell time (t_{OL}).

Condition	1	2	3	4
OLF	1.05	1.15	1.05	1.15
t_{OL} (s)	1	1	10	10

Fig. 8 illustrates the stress-distance profiles generated at different time points for the OL condition 3 (OLF = 1.05, t_{OL} = 10s) simulated with σ_{dwell} of 300 MPa. Upon initial loading (at t_1 = 1s when σ_{OL} is first reached) the stress distribution (in orange) features similar characteristics to dwell-only (standard) stress profiles. Local crack opening stresses peak at short distance ahead of the crack-tip with a steep decrease in stress levels towards the crack-tip. Note that also here (as observed in behaviour during dwell-only loading) the constitutive response is modelled through a microstructure explicit rate-dependent formulation, resulting in stress relaxation ahead of the crack tip. However, upon partially unloading from the overload condition (σ_{OL} to σ_{dwell}), stress-distance profiles change significantly in shape with σ_{22} reducing preferentially close to the crack-tip. Therefore, reductions in local tensile stresses immediately ahead of the crack-tip are markedly larger than the percentage of unloading applied. **Fig. 8** also highlights that, in particular, near crack-tip stresses change appreciably with dwell time, while stress fields further away/ahead from the crack-tip (distance > 2 μm) are relatively flat with subtle differences only in σ_{22} for different hold (dwell) times.

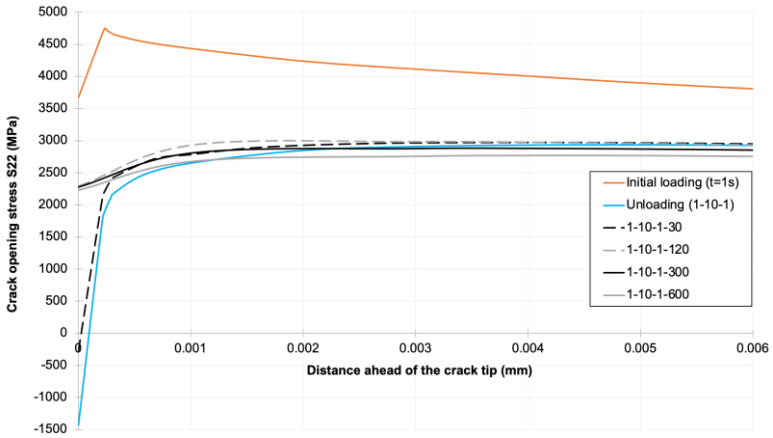

Fig. 8: Stress-distance profiles at different dwell times for the FE model subjected to σ_{dwell} = 300 MPa, OLF = 1.05 and t_{OL} = 10s.

328

329 **Fig. 9** compares local crack-tip opening stress fields as a function of distance (up to 2 μm ahead
330 of the crack-tip) for simulations run under: standard (STD) dwell; 1s OL; and 10s OL loading conditions
331 with σ_{dwell} = 300 MPa and OLF = 1.05. Each graph (a-c) is plotted for a specific dwell time (30, 120 and
332 300s respectively) and, in each case, local stress-distance profiles for the three different loading
333 conditions can be compared at similar moments in time. For t_{dwell} = 30s (**Fig. 9(a)**), neither 1s nor 10s
334 OL stress curves (1-1-1-30 and 1-10-1-30) have re-joined the STD dwell curve (1-30). For both OL
335 conditions, near-tip stresses are recovering towards their non-overload level with σ_{22} even being
336 compressive for 1-10-1-30 (-280 MPa at the crack-tip). For t_{dwell} = 120s (**Fig. 9(b)**), local stress states
337 associated to 1-120 and 1-1-1-120 are now predicted to be essentially identical (at the crack-tip: 2455
338 and 2450 MPa respectively). In contrast for 1-10-1-120, tensile stress levels are still appreciably lower
339 (2290 MPa). The effect of overloads on near-tip stress recovery seems to reduce more gradually for t_{OL}
340 = 10s compared to t_{OL} = 1s. At t_{dwell} = 300s (**Fig. 9(c)**), all three stress curves have converged and local
341 crack-tip stress fields for 10s OL appear to have now also fully recovered back to their "unloaded state".
342 These results suggest that, during a first portion of subsequent dwell time, local crack-tip stresses from
343 simulated OL cycles relax back towards their standard dwell (non-overload) stress state, whilst
344 neighbouring stress fields redistribute. However, with longer hold times, crack-tip stress recovery
345 diminishes as local stress states converge, and thereafter normal dwell effects will resume (i.e. σ_{22}
346 profiles are progressively lowered with prolonged dwell).
347

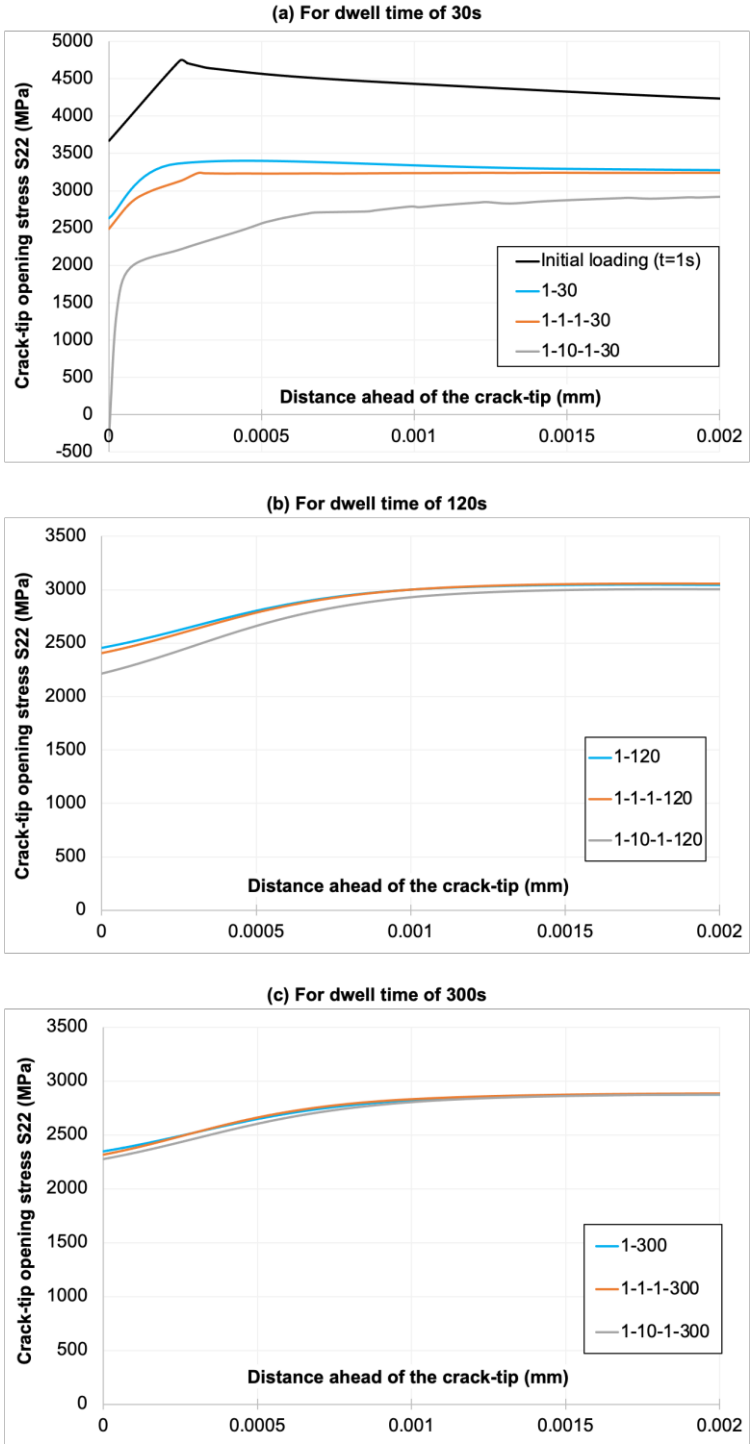

Fig. 9: Local stress-distance profiles compared for standard dwell, 1s and 10s overload condition (σ_{dwell} = 300 MPa and OLF = 1.05) (a) t_{dwell} = 30s, (b) t_{dwell} = 120s, (c) t_{dwell} = 300s.

To characterise the entire local crack-tip stress field evolution with dwell time, crack-opening stresses are tracked against time at an individual node very close to the crack-tip. Here, the first node ahead of the modelled crack-tip (5 nm away) was chosen. Since this node is very local to the crack-tip,

355 stress data extracted from this node is presumed to characterise crack-opening stress levels essentially
356 at the crack-tip. **Fig. 10** represents the crack-tip stress-time histories generated for all four simulated
357 OL conditions and compares them against the standard dwell relaxation curve (in red). Note that the
358 time axis captures the onset of non-overload dwell allowing stress-time histories to be compared at
359 similar times during subsequent dwell. At the start of dwell, crack-tip σ_{22} predicted for OL simulations
360 are markedly lower, or as is the case for some conditions approach zero, or even become strongly
361 compressive (-3700 MPa). Over time, these local crack-tip stress fields slowly relax back towards
362 normal dwell stress levels.

363 There is a prominent difference in how quickly local tensile stresses recover back to their non-
364 overload level, strongly dependent on both OLF and t_{OL}. For illustrative purpose, an engineering
365 approximation is next adopted to introduce an incubation time (t_{inc}) defined as the time it takes upon
366 unloading for crack-tip stresses at this node to recover to within 2% of the local stress at this node under
367 relaxation from a standard dwell hold. Numerically-derived incubation times (**Table 5**) increase with
368 higher OLF and longer t_{OL}. Extended OL dwell (10s) as well as larger OL (15%) produce larger
369 compressive stress fields close to the crack-tip and so it takes longer for stresses to recover back which
370 translates into increased t_{inc}. Note that higher values of K result in slightly shorter t_{inc} which implies a
371 slightly reduced OL effect. Modelling even predicts that for OL No. 4 condition (OLF = 1.15 and t_{OL} =
372 10s) crack-tip σ_{22} will never fully recover even after a one-hour dwell cycle.
373
374 **Table 5:** Incubation times, as captured by FE simulations, are presented for all four overload conditions
375 simulated for two different applied K values

Condition	**1** t_{OL} = 1s OLF = 1.05	**2** t_{OL} = 1s OLF = 1.15	**3** t_{OL} = 10s OLF = 1.05	**4** t_{OL} = 10s OLF = 1.15
t_{inc} (s) for K = 21.7 MPa.m$^{1/2}$	40	2540	290	>3,600
t_{inc} (s) for K = 32.6 MPa.m$^{1/2}$	25	1430	240	>3,600

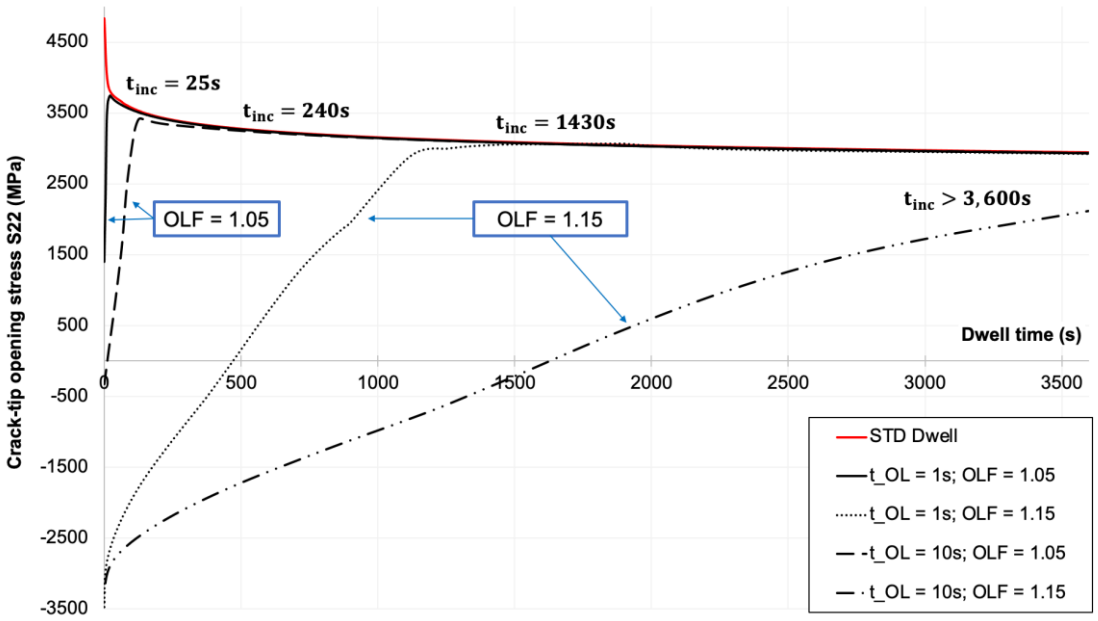

Fig. 10: Crack-tip stress-time histories (σ_{22} versus non-overload dwell time) are generated at the first node ahead of the modelled crack-tip and compare four different overload conditions with the standard (STD) dwell loading case (for σ_{dwell} = 300 MPa).

4. Discussion

Although crack growth testing has led to the development of empirically-based predictive models, research has not been able to produce many conclusive results on local crack-tip phenomena involved during failure mode interactions of cycle- and time-dependent processes [3, 5, 6]. Oxidising environments have long been recognised to cause accelerated FCGR (da/dN) in air, especially under dwell conditions, as a result of intergranular crack growth [6-13]. However, during prolonged dwell periods, creep strain accumulation (due to time-dependent plasticity) can lead to stress relaxation effects in the vicinity of the crack-tip which have been seen to play a beneficial role in retarding intergranular crack growth mechanisms [17, 18]. Under extreme conditions (overload), time-dependent plasticity might develop to such extent that the crack can no longer advance by oxide cracking, thereby switching off the environmentally-enhanced crack growth mechanism during the dwell period [9, 22]. Note that at particular high temperatures (>750°C), creep damage processes characterised by intergranular micro-

void coalescence can start to dominate in both air and vacuum environments and may also lead to accelerated FCGR during dwell periods [4, 16]. Furthermore, microstructural changes arising during prolonged thermal exposures can also control plasticity responses [8]. In this current paper, the effects of oxidation and plasticity are decoupled to focus on local mechanical stress fields due to (time-dependent) plasticity alone. The rationale for performing stress-based FE modelling to investigate time-dependent plasticity is ascribed to the significance of stress modifications in the crack-tip region for characterising DFCG. The following discussion attempts to address how numerical models may draw some insight on dwell crack growth mechanisms (and controlling parameters).

4.1. Dwell effects

A comprehensive (time-dependent) constitutive creep model is utilised here to carry out stress-based FEA on a 2D cracked geometry. Computed stress-distance profiles (for example, in **Fig. 6**) show that the introduction of dwell periods can lead to local stress relaxation, which has experimentally been reported to beneficially influence DFCG behaviour either by reducing FCGR or even promoting crack arrest [7, 17, 18]. Predicted peak tensile stresses are 4775 and 4740 MPa for applied linear elastic stress intensity factors of 21.7 and 32.6 MPa.m$^{1/2}$ respectively at a time of one second. These are similar to those that can be calculated from an earlier (time-independent plasticity) analysis reported by McMeeking [32]. During dwell, the crack-tip region accumulates more creep strain which causes tensile stresses to further relax local peak stresses and their decay with distance from the crack-tip. It is also of note that crack-tip blunting is predicted to occur (**Fig. 7**). For example, over a 3600s dwell period, the CTOD is predicted to increase from 1.2 and 2.4 μm (upon initial loading) to 1.5 and 3.4 μm, for σ_{dwell} of 200 and 300 MPa respectively. Although these are relatively modest increases in CTOD in absolute terms, they are still considered to have potential to promote crack growth retardations, and such retardations are routinely seen experimentally at lower ranges of applied stress intensity factors [15, 16].

In light of the data simulations, creep micro-mechanisms operate in very local regions around the crack-tip. Dwell effects were shown to be lost in the far-field material and physical distances

421 governing the action of plasticity were predicted to lie within the micron-scale. A physically-based
422 approach for characterising near crack-tip behaviour uses the CTOD parameter. Crack blunting (due to
423 local creep deformation) affects a zone of a few CTOD ahead of the crack-tip. With longer hold (dwell)
424 times, this 'damage zone' is pushed forward and the extent of the relaxed stress fields spreads. On the
425 basis of time-dependent plasticity only (assuming no creep damage can occur in crack-tip regions),
426 standard dwell simulations predict that the local crack-tip stress state becomes less damaging with
427 increasing dwell time. Since crack-opening stress fields are decaying over time, driving forces for crack
428 growth are lowered which potentially reduces FCGR and thus fracture becomes more and more
429 unlikely. So, for example, if no crack growth is observed over a dwell cycle 1-300-1-1, then based
430 purely on the stress relaxation (and a fracture criterion of maximum local stress) no crack growth is to
431 be expected over a longer dwell cycle of, for example, 1-600-1-1. Note that some caution should be
432 exercised if this approach is ever to be extended to components which can be subjected to significant
433 net section stresses and where ("bulk") creep may occur.
434 However, high-temperature material degradation due to oxidation majorly contributes to crack
435 growth (i.e. accelerated DFCGR) and will inevitably influence the potential for fracture (due to GB
436 embrittlement and oxide breaking). So, the overall description for DFCG needs to account for oxide
437 growth and its influence on local stress states. Detailed calculations [19] of oxide formation ahead of a
438 crack-tip under stressed and stress-free conditions have shown that compressive stress states develop in
439 the oxide. Compressive stresses gradually decrease and become tensile with further distance away from
440 the crack-tip towards the front end of the oxide. These stress states then become significantly more
441 important in magnitude as the oxide grows and thus failure will eventually occur. Here, the "paradox"
442 is that local stress fields become less damaging (more relaxed) as dwell time increases but longer dwell
443 times are more damaging because they are observed to result in increased crack growth rates (da/dN).
444 Moreover, it is apparent that immediately at the beginning of dwell periods the oxide will be under the
445 least compression when at its thinnest and local tensile stresses are at their highest (in the crack-tip
446 region) because they have not yet relaxed as much. Hence, logic claims that fracture cannot be defined
447 by a unique stress at a unique point since otherwise the oxide is predicted to break straightaway at the
448 start of the dwell period. Clearly due to the complexity associated with the interactions of the time-

449 dependent mechanisms of oxide growth and time-dependent stress relaxation, a stress-based analysis
450 on its own is insufficient to derive an absolutely precise fracture criterion.
451
452 ## 4.2. Overload effects
453 The motivation to investigate overload cycling conditions comes from the need to more accurately
454 model engine flight profiles in order to improve lifing strategies. Overload waveforms better represent
455 in-service stress states; they describe partial unloading from maximum to dwell load which replicates
456 the switch in engine capacity from "take-off" to "climb" events during typical flight cycles. Crack
457 growth retardation phenomena have experimentally been observed to occur when partially unloading
458 from higher stress conditions (overload) [9, 13, 18, 21-23]. For fatigue cycling, several mechanisms
459 (crack blunting, branching, strain-hardening, crack-tip closure) have been proposed in an attempt to
460 rationalise crack growth retardation. Despite some discrepancies, they all emphasise the importance of
461 local crack-tip stress fields. For dwell cycling, the most relevant concept postulates that the preferential
462 unloading of crack-tip stresses leads to significant changes in near-tip stress levels which introduce
463 residual zones ahead of the crack-tip [21, 22].
464 In this current paper, FEA modelling of overload conditions has revealed two distinctive
465 features with important implications on DFCG behaviour. Significant reductions in local tensile stresses
466 induce a compressive (residual) stress zone just ahead of the crack-tip which effectively lowers crack
467 driving forces. Secondly, large near-tip stress relaxation driven by active creep mechanisms occurs
468 during subsequent dwell periods. Stress relaxation effects are associated with inelastic creep strain rates
469 near the crack-tip which may delay intergranular damage processes. Altogether, this sensibly explains
470 how overload cycling conditions may reduce FCGR or in some cases even promote crack arrest. This
471 current paper specifically studies and compares the crack-tip stress field criterion under standard dwell
472 and overload conditions. The beneficial effect of OL on (potential) crack growth retardation reduces
473 over time as crack-opening stress fields recover back from their "unloaded" state. Therefore, it is natural
474 to reason that there is an incubation time associated to each OL condition which defines the time it takes
475 for local crack-tip stresses to converge back to identical stress states under both loading cases. The

incubation time characterises the extent of crack growth retardation and is here derived by applying an engineering approximation which relies on the basis of matching crack-tip stress relaxation curves computed for overload and dwell-only simulations within a 2% difference. A key differentiation between 'partial' and 'full' retardation is established as outlined below and correlates well to similar classifications presented in previous studies [9]:

(i) If $t_{inc} < t_{dwell}$: crack growth is inhibited whilst near-tip stresses are recovering towards their non-overload (dwell) level. Once local tensile stresses have fully relaxed back *at* $t_{inc} = t_{dwell}$ time-dependent crack growth will resume as usual for the remainder of the dwell period (resulting in partial retardation) and thereafter response to crack growth mechanisms is identical;

(ii) If $t_{inc} > t_{dwell}$: near-tip stresses will never relax back to their non-overload (dwell) level within one simulated cycle. Time-dependent components of crack growth are completely lost, and full retardation must be achieved back to fatigue baseline rates (which are controlled primarily by the stress intensity factor range).

A noteworthy finding of the presented modelling work is that the extension of overload dwell time (t_{OL}) from 1 to 10 seconds leads to a minimum six-fold increase in incubation time. The model suggests that 1s OL does not significantly affect local crack-opening stress states (compared against STD dwell) whereas 10s OL beneficially reduces near crack-tip stress levels which may even become compressive. For longer holds at OL, more extensive creep strain accumulates around the crack-tip which results in crack-tip stresses relaxing back more slowly as creep strain evolution approaches a steady state. FEA modelling predicts that a 240s incubation time associated with 1-10-1-300 delays time-dependent crack growth so that, instead of having the full dwell effect of 300s, only 60s of dwell are contributing. Yet, modelling results do not capture that even a short (1s) and small (5%) OL have been observed to reduce FCGR compared to those associated with dwell-only loading [9, 18].

The methodology of analysis used in the current paper relies on the selection of specific dwell times and particular nodes within the post-processing module of ABAQUS. This inevitably leads to a weakness in the calculation of incubation times which are performed at an individual point (here at the

first node 5 nm ahead of the crack-tip). Indeed, it has been shown that the peak in crack-opening stress distribution reduces and moves further ahead with time under standard dwell conditions **(Fig. 6)**, precise incubation times may differ slightly if local stresses are interrogated at other nodes further ahead of the crack-tip. Thus, the model as presented here captures the mechanics of the crack-tip stress field (in the absence of any oxide present) accurately at the point interrogated. In addition, the influence of oxide growth on local stress states has not been considered and so it is difficult to determine an absolute value for a fracture stress criterion from this modelling work alone. This paper has however demonstrated the importance of local stresses around the crack-tip when relating overload effects and time-dependent plasticity.

As many mechanisms compete and combine to influence DFCG behaviour, it is important to highlight that the complete story of overload effects should be concerned with whether intergranular cracking occurs during overload hold (at σ_{OL}) due to time-dependent oxide formation and subsequent embrittlement of the GB. Even if local tensile stresses take longer to recover when extended OL periods (such as 10s) are applied, potential retardation could be overly optimistic if crack growth can occur during the OL dwell period (such as 10s) itself.

In regards to component integrity assessments, the mechanisms involved during OL cycling and associated retardation phenomena still require a comprehensive and complete description. The extent of large reductions in FCGR has important implications on lifing strategies. Based on the importance of crack-tip stresses and time-dependent plasticity, computational techniques as presented in this paper have allowed insight into how overloads can lead to significant retardation effects. Current lifing approaches are still extremely conservative and understanding aided by numerical modelling has potential to extend certified life in aero-engine turbine discs.

5. Conclusions

A detailed numerical creep model based on microstructural variables has successfully been implemented. Numerical outputs from the FE model, considering time-dependent plasticity and subjected to standard dwell and overload cycles, represent the basis for performing a stress-based

analysis of the development of mechanical fields ahead of the crack-tip. The main conclusions are summarised as follows.

1. FEA modelling has provided insight into DFCG behaviour by considering effects of time-dependent plasticity. Here, it particularly adds confidence to the underlying mechanism of stress relaxation arising from such time-dependent plasticity and illustrates how rapidly local crack-tip stresses can relax.
2. The local refined mesh has been validated against the rationale of physical distances (micro-scale) involved in controlling the action of time-dependent processes. FEA results considered after initial loading (at a time of one second) have also shown good correlation with previous (time-independent) plasticity analysis in terms of both the value and location of local peak stress values.
3. Introduction of dwell periods leads to near-tip stress relaxation by time-dependent plasticity. With increasing hold times, a larger zone ahead of the crack-tip is affected by crack-tip blunting and the extent of relaxed stress fields is pushed forward due to creep strain accumulation.
4. The beneficial characteristics of overloads are reasonably well captured. FE simulations are able to identify (i) the compressive stress fields which lower crack driving forces and (ii) the large near-tip stress relaxation. A numerically-derived incubation time has successfully been applied in predicting the general trends of achieving more pronounced retardation effects with larger overload factors and extended overload dwell. FEA modelling predicts a significant difference in behaviour between a 1s and 10s overload period.
5. Modelling work has given insight into the existing competition between oxide growth and plasticity. The importance of studying local crack-tip stress fields in regards to DFCG has been emphasised. It is plausible to conclude that the main characteristics for applications to lifing could be captured on the basis of crack-tip stresses by plasticity only. A precise definition of a physically-based fracture criterion for oxide failure under dwell loading still remains a future challenge**.**

Acknowledgments

The authors are grateful for the support of this work by Rolls-Royce. The present work was carried out at the Rolls-Royce University Technology Center at the University of Birmingham in the framework of a final year (master's) project.

References

1. Hardy MC, Zirbel B, Shen G, Shankar R. Developping damage tolerance and creep resistance in a high strength nickel alloy for disc applications. *TMS: Superalloys 2004*. 2004:83-90.
2. Reed RC. *The superalloys: fundamentals and applications*: Cambridge University Press; 2006.
3. Knowles DM, Skelton DK. High temperature fatigue of a polycrystalline nickel base superalloy. *Materials Science and Technology*. 2001;17(11):1403-1412.
4. Knowles DM, Hunt DW. The influence of microstructure and environment on the crack growth behavior of powder metallurgy nickel superalloy RR1000. *Metallurgical and Materials Transactions*. 2002;A33:3165-3172.
5. Pineau A, Antolovich SD. High temperature fatigue of nickel-base superalloys - A review with special emphasis on deformation modes and oxidation. *Engineering Failure Analysis*. 2009;16:2668-2697.
6. Yu SY, Li HY, Hardy MC, McDonald SA, Bowen P. Mechanisms of dwell fatigue crack growth in an advanced nickel disc alloy RR1000. *MATEC Web of Conferences*. 2014;14.
7. Liu X, Kang B, Chang KM. The effect of hold-time on fatigue crack growth behaviors of WASPALOY alloy at elevated temperature. *Materials Science and Engineering*. 2003;A340:8-14.
8. Turan D, Hunt D, Knowles DM. Dwell time effect on fatigue crack growth of RR1000 superalloy. *Materials Science and Technology*. 2007;23(2):183-188.
9. Fisk JC. Effects of creep and oxidation interaction on high temperature crack growth behaviour of nickel based superalloys: University of Birmingham; 2013.

10. Pang HT, Hardy MC, Hide N, Wilcock IM, Henderson MB, Reed P. Comparison of fatigue crack propagation in nicel base superalloys RR1000 and Udimet 720Li. *Materials Science and Technology*. 2016;32(1):22-39.
11. Ghonem H, Nicholas T, Pineau A. Elevated temperature fatigue crack growth in alloy 718 - Part II: Effects of environmental and material variables. *Fatigue and Fracture of Engineering Materials and Structures*. 1993;16(6):557-590.
12. Onofrio G, Osinkolu GA, Marchionni M. Fatigue crack growth of UDIMET 720 Li superalloy at elevated temperature. *International Journal of Fatigue*. 2001;23:887-895.
13. Gustafsson D, Lundström E. High temperature fatigue crack growth behaviour of Inconel 718 under hold time and overload conditions. *International Journal of Fatigue*. 2013;48:178-186.
14. Evans HE, Li HY, Bowen P. A mechanism for stress-aided grain boundary oxidation ahead of cracks. *Scripta Materialia*. 2013;69:179-182.
15. Kitaguchi HS, Li HY, Evans HE, Ding RG, Jones IP, Baxter G, et al. Oxidation ahead of a crack tip in an advanced Ni-based superalloy. *Acta Materialia*. 2013;61:1968-1981.
16. Li HY, Sun JF, Hardy MC, Evans HE, Williams SJ, Doel TJA, et al. Effects of microstructure on high temperature dwell fatigue crack growth in a coarse grain PM nickel based superalloy. *Acta Materialia*. 2015;90:355-369.
17. Telesman J, Gabb TP, Ghosn LJ. Separating the Influence of Environment from Stress Relaxation Effects on Dwell Fatigue Crack Growth in a Nickel-Base Disk Alloy. 13th International Symposium on Superalloys; Seven Springs (United States): Minerals, Metals and Materials Society; 2016.
18. Telesman J, Gabb TP, Ghosn LJ. A novel methodolody for modeling dwell fatigue crack growth in Ni-based superalloys. *International Journal of Fatigue*. 2020;133.
19. Fang CZ, Basoalto HC, Anderson MJ, Li HY, Williams S, Bowen P. A numerical study of the influence of grain boundary oxides on dwell fatigue crack growth of a nickel-based superalloy. *Journal of Materials and Technology*. 2021;104, 30 March 2022: 224-235 (published online 08/09/2021).

20. Molins R, Hochstetter G, Chassaigne JC, Andrieu E. Oxidation effects on the fatigue crack growth behaviour of alloy 718 at high temperature. *Acta Materialia*. 1997;45(2):663-674.
21. Ponnelle S, Brethes B, Pineau A. High temperature fatigue crack growth rate in Inconel 718: Dwell effect annihilations. *European Structural Integrity Society*. 2002;29:257-266.
22. Telesman J, Gabb TP, Kantzos P, editors. Effect of overloads on time dependent fatigue crack growth in a nickel based superalloy. *International Fatigue Congress* 2002; Stockholm (Sweden).
23. Saarimäki J, Moverare J, Eriksson R, Johansson S. Influence of overloads on dwell time fatigue crack growth in Inconel 718. *Materials Science and Engineering*. 2014;A612:398-405.
24. Reed RC, CMF R. 22.5.4. Model for composition dependence of creep deformation. Physical Metallurgy: 22 - Physical Metallurgy of the Nickel-Based Superalloys: Elsevier; 2014. p. 2215-2290.
25. Orowan E. The Creep of Metals. *Journal West of Scotland Iron and Steel* 1946-1947;54:45-96.
26. Dyson BF. Microstructure based creep constitutive model for precipitation strengthened alloys: theory and application. *Materials Science and Technology*. 2009;25(2):213-220.
27. Basoalto HC, Sondhi SK, Dyson BF, McLean M. A generic microstructure explicit model of creep in nickel-base superalloys. *TMS: Superalloys 2004*. 2004:897-906.
28. Basoalto HC, Brooks JW, Di Martino I. Multiscale microstructure modelling for nickel based superalloys. *Materials Science and Technology*. 2009;25(2):221-227.
29. Coakley J, Dye D, Basoalto H. Creep and creep modelling of a multimodal nickel-base superalloy. *Acta Materialia*. 2011;59(3):854-863.
30. ABAQUS, Version 6.13 User's manual, SIMULIA, Providence, RI, 2013 [Internet]. Simulia.
31. Standard Method of Test for Plane-Strain Fracture Toughness of Metallic Materials (Designation: E 399-72), *Annual Book of ASTM Standards, 1972,* Part 31, pp. 955-974.
32. McMeeking RM. Finite deformation analysis of crack-tip opening in elastic-plastic materials and implications for fracture. *Journal of Mechanical Physical Solids*. 1977;25:357-381.

Figure Legends

Fig. 1: Three typical examples of engine loading cycles: baseline cycling, dwell cycling, and overload cycling.

Fig. 2: Crack growth resistance curves (da/dN vs ΔK_{full}) showing an example of dwell and overload-dwell effects on DFCG behaviour in LSHR alloy at 704°C [18].

Fig. 3: Schematic illustration showing the variation in normal out-of-plane stress along oxide intrusion ($0 \leq x \leq l$) in the absence of an applied load [14].

Fig. 4: Schematic of the boundary conditions applied to the 2D SENT specimen geometry. Illustration of the implemented 2D FE mesh in ABAQUS. Global mesh with coarse mesh and a locally refined mesh near the crack-tip [19].

Fig. 5: Simulated loading waveforms **(a)** The standard dwell cycle is modelled as 1-t_{dwell} stress waveform: initial stress ramp-up to σ_{dwell} in 1s (t_1) and hold at σ_{dwell} for t_{dwell}. **(b)** The overload cycle is modelled as 1-t_{OL}-1-t_{dwell} stress waveform: initial stress ramp-up to σ_{OL} in 1s (t_1), hold at overload until t_2 (t_2 - t_1 denotes the overload dwell time), unload from σ_{OL} to σ_{dwell} in 1s (t_3) and normal hold at σ_{dwell} for t_{dwell}.

Fig. 6: Stress-distance profiles at different points for the FE model (RR1000 at 650°C) subjected to simulated dwell-only cycles with σ_{dwell} of 300 MPa. Stress distribution plotted in regards to crack-tip opening stress S22 and S22 normalised by the yield stress (σ_y = 1000 MPa).

Fig. 7: Crack-tip opening displacement plotted versus time, with CTOD/2 numerically investigated at the CTO-node selected (2 μm behind the crack-tip).

Fig. 8: Stress-distance profiles at different time points (dwell times) for FE model subjected to σ_{dwell} = 300 MPa, OLF = 1.05 and t_{OL} = 10s.

Fig. 9: Local stress-distance profiles compared for standard dwell, 1s and 10s overload condition (σ_{dwell} = 300 MPa and OLF = 1.05) (a) t_{dwell} = 30s, (b) t_{dwell} = 120s, (c) t_{dwell} = 300s.

Fig. 10: Crack-tip stress-time histories (σ_{22} versus non-overload dwell time) are generated at the first node ahead of the modelled crack-tip and compare four different overload conditions with the standard (STD) dwell loading case (for σ_{dwell} = 300 MPa).